Model-Guided Development of Advanced, Low Cost Anion-Exchange Membrane Fuel Cells

Assoc. Prof. Dario Dekel

Department of Chemical Engineering – Technion – IIT

Advancement Report

The Melvin & Caroline Miller Novelty Fund

Submitted to VP Research, Technion – IIT

June 2019

A. Abstract

The research has focused on designing and testing anion-exchange membrane fuel cells (AEMFCs). The results mentioned herein include a novel, milestone model of AEMFC performance stability, and additional conclusions on anion-exchange membranes' (AEM) behavior in realistic, CO_2-containing air. These results have been published in peer-reviewed papers – attached below as-is. The preparation of non-Pt electrodes and their testing in fuel cells has not been published yet and is presented in the following section.

B. Non-Pt AEMFC Testing

We have prepared two types of non-Pt anodes (AN), and used the same, non-Pt, N-doped carbon cathode (CA). The two anodes were a NiFe and a Pd-CeO_2. The IV (polarization) curves and both settings are presented below.

1. NiFe

Anode - Catalyst Coated Membrane (CCM): 4.135 mg_{NiFe}/cm^2 on A-201 with AS-4 ionomer (50:50 AEI to catalyst ratio)

Cathode – Gas Diffusion Electrode (GDE): 0.703 $mg_{N\text{-}doped\text{-}C}/cm^2$ with TMA-functionalized Fumatech ionomer (30:70 AEI to catalyst ratio)

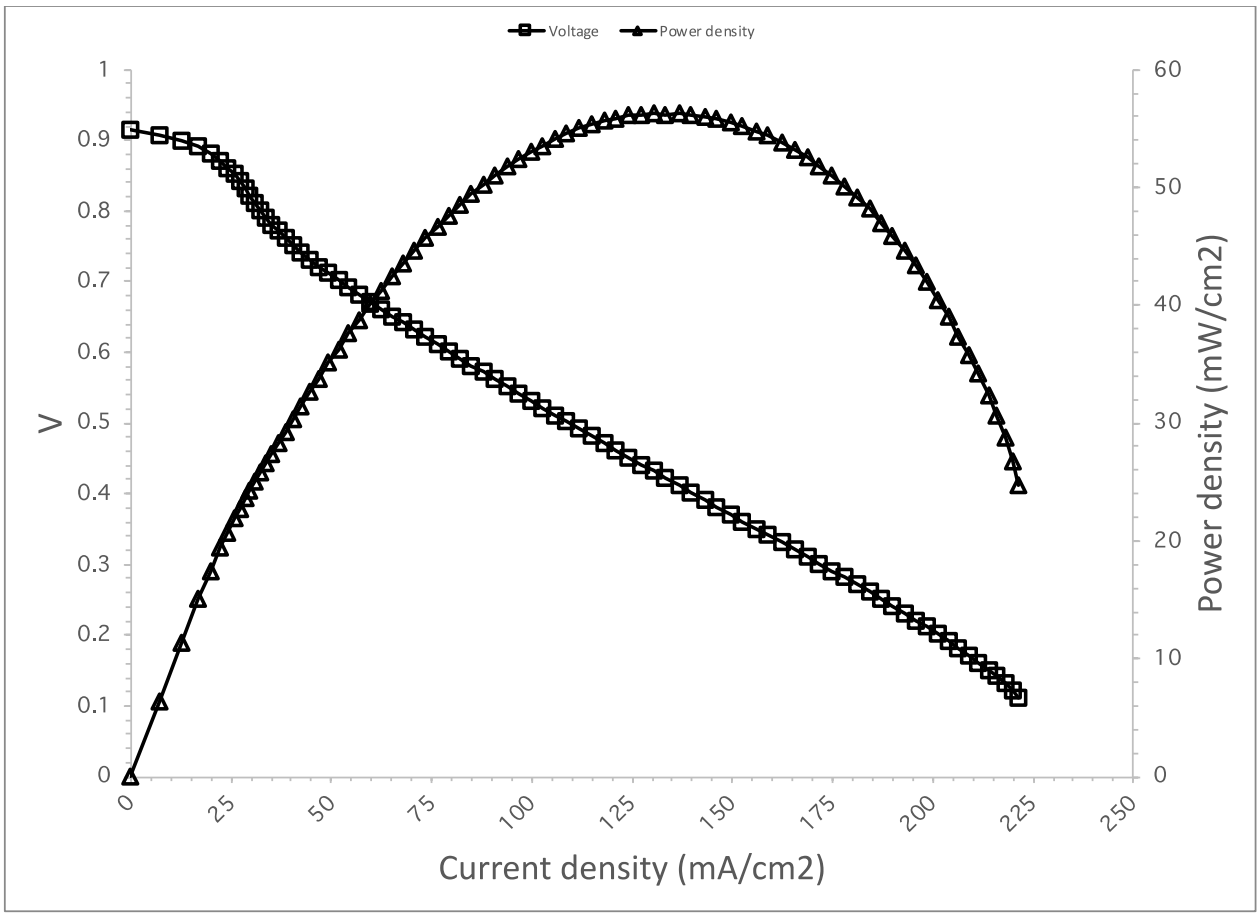

AN: DP = 95°C, Inlet = 95°C, Flow = 0.01 SLPM, RH = 100%, Pressure=2 bar_a
CA: DP = 95°C, Inlet = 95°C, Flow = 0.2 SLPM, RH = 100%, Pressure = 0 bar_a
Cell temp = 95°C

The activity of this catalyst combination seems to be quite poor, mainly due to the novel, NiFe catalyst as the next results show. Still, it does present some activity, and further development of this promising catalyst is underway.

2. $Pd\text{-}CeO_2$

AN GDE: 0.719 mg_{PdCeO2}/cm^2 with TMA-functionalized Fumatech ionomer (20:80 AEI to catalyst ratio)

CA GDE: 0.703 $mg_{N\text{-}doped\text{-}C}/cm^2$ with TMA-functionalized Fumatech ionomer (30:70 AEI to catalyst ratio)

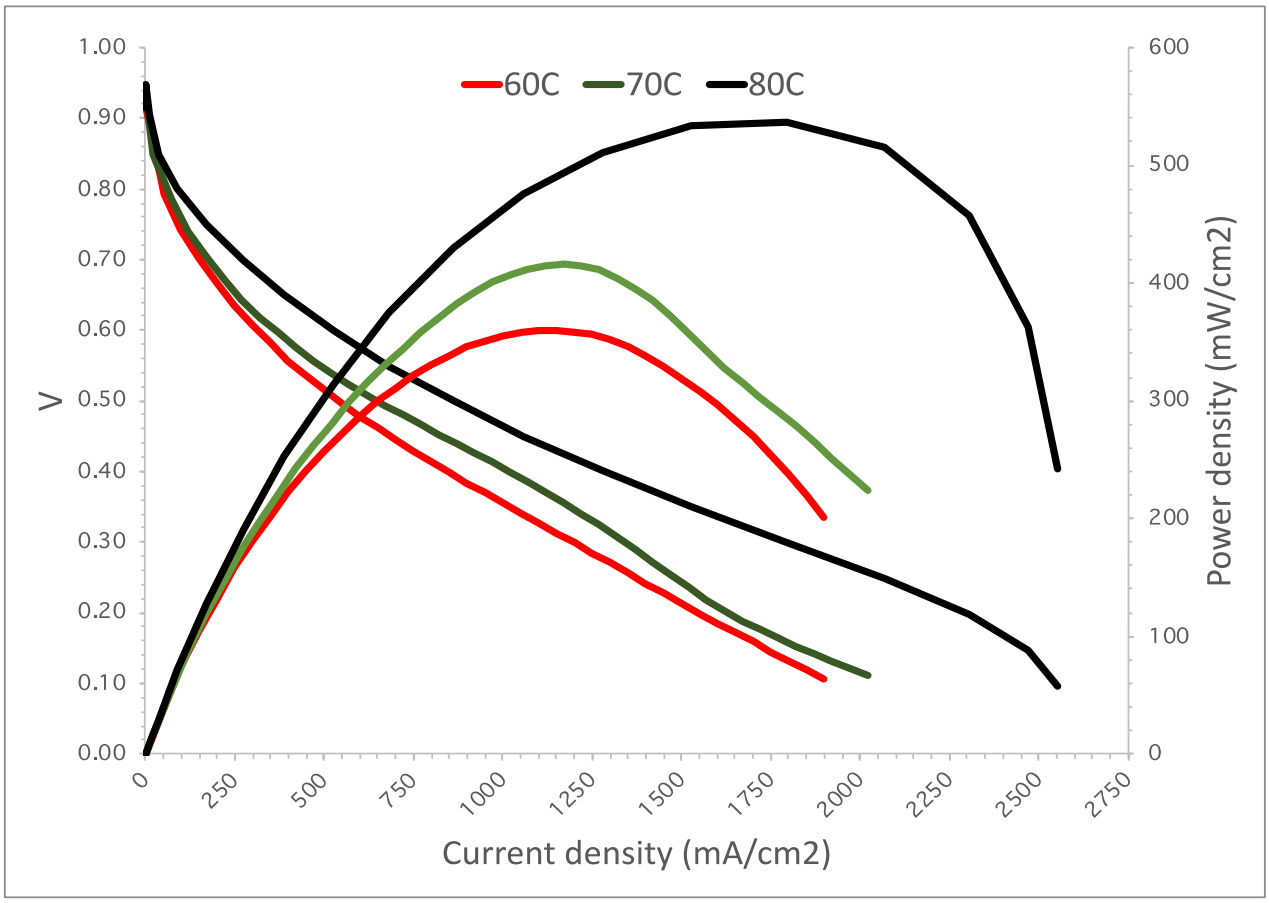

AN DP = 55 °C Inlet = 60 °C Flow = 1 SLPM RH = 79% BP = 0 bar_a **CA** DP = 57 °C Inlet = 60 °C Flow = 1 SLPM RH = 86% BP = 0 bar_a Cell temp = 60 °C	**AN** DP = 65 °C Inlet = 70 °C Flow = 1 SLPM RH = 80% BP = 2 bar_a **CA** DP = 67 °C Inlet = 70 °C Flow = 1 SLPM RH = 88% BP = 0 bar_a Cell temp = 70 °C	**AN** DP = 75 °C Inlet = 80 °C Flow = 1 SLPM RH = 82% BP = 2 bar_a **CA** DP = 77 °C Inlet = 80 °C Flow = 1 SLPM RH = 89% BP = 2 bar_a Cell temp = 80 °C

This catalyst combination, including the proven Pd-CeO_2 anode catalyst and the N-doped carbon catalyst shows good results in a wide range of operation temperatures, and in different pressure combinations. The relative humidity (RH) is not set to the maximum, following modeling inputs (See below in the published paper).

C. Published papers (from the next page)

1. "Predicting performance stability in anion exchange membrane fuel cells"; Dario R. Dekel, Igal G. Rasin and Simon Brandon; J. Power Sources, 420, 118-123, **2019**.
2. "Effect of CO_2 on the properties of anion exchange membranes for fuel cell applications"; Noga Ziv, Abhishek N. Mondal, Thomas Weissbach, Steven Holdcroft and Dario R. Dekel; J. Membrane Sci. 586, 140-150, **2019**.

Journal of Power Sources 420 (2019) 118–123

Contents lists available at ScienceDirect

Journal of Power Sources

journal homepage: www.elsevier.com/locate/jpowsour

Short communication

Predicting performance stability of anion exchange membrane fuel cells

Dario R. Dekel[a,b,*], Igal G. Rasin[a], Simon Brandon[a,b,*]

[a] The Wolfson Department of Chemical Engineering, Technion – Israel Institute of Technology, Haifa, 3200003, Israel
[b] The Nancy & Stephan Grand Technion Energy Program (GTEP), Technion – Israel Institute of Technology, Haifa, 3200003, Israel

HIGHLIGHTS

- We present a unique model capable of predicting the performance stability of AEMFCs.
- The model relates between ionomer degradation, hydration and operating conditions.
- Model results provide critical insights for the development of highly stable AEMFCs.
- Using AEMs with achievable targeted properties, the model predicts life-time > 5000h

GRAPHICAL ABSTRACT

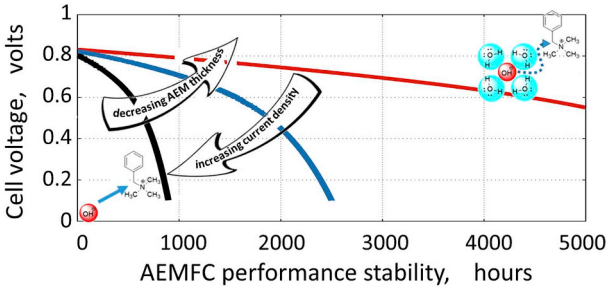

ARTICLE INFO

Keywords:
Anion exchange membrane fuel cells
Modeling
Hydration
Membrane degradation
Ionomer degradation
Cell performance stability

ABSTRACT

Anion-exchange membrane fuel cells (AEMFCs) are attracting increasing attention worldwide mainly due to this technology's potential to considerably reduce fuel cell device costs. However, their development and implementation is significantly handicapped by the membrane and ionomer's decomposition during cell operation. In this study we propose and apply a unique one-dimensional model capable of predicting, for the first time, the performance stability of AEMFCs. The model accounts for the ionomeric material degradation and its relationship with local hydration, which depends on cell material properties, design parameters and operating conditions. Using this model, we successfully demonstrate the strong impact of operating current density and membrane characteristics on the performance stability of a representative cell. The predicted cell stability provides critical insights for the design and development of highly stable AEMFCs. By using membranes with achievable targeted properties, the model predicts an AEMFC life-time higher than 5000 h, suitable for automotive applications.

1. Introduction

The growing interest [1] in anion exchange membrane fuel cells (AEMFCs) is driven by the potential advantage of these systems over the relatively established proton exchange membrane fuel cells (PEMFCs). These advantages include superior oxygen reduction reaction (ORR) kinetics due to the high pH conditions, enabling the use of relatively cheap Pt-free catalysts [1–9], and reduced fuel crossover due to the use of hydrocarbon-based anion exchange membranes (AEMs) [1,10]. As a result of these strengths (relative to PEMFCs), AEMFCs can potentially revolutionize the fuel cell market, particularly for automotive applications, where fuel cell stack costs are critical.

The large effort invested in hydrogen AEMFC research has recently led to substantial advances in cell performance in these systems, as was recently summarized in a review study [11]. Achievements include peak power densities and limiting current densities equal to or larger than 1.0 W cm^{-2} and 2.0 A cm^{-2}, respectively [11], both with Pt-based catalysts [12–14] and without Pt [2–5,15]. However, despite these

* Corresponding authors. The Wolfson Department of Chemical Engineering, Technion – Israel Institute of Technology, Haifa, 3200003, Israel.
E-mail addresses: dario@technion.ac.il (D.R. Dekel), cersbsb@technion.ac.il (S. Brandon).

https://doi.org/10.1016/j.jpowsour.2019.02.069
Received 20 October 2018; Received in revised form 19 February 2019; Accepted 20 February 2019
Available online 08 March 2019
0378-7753/

significant achievements, cell performance is found to be unstable, reducing over time in a manner that currently limits the most advanced AEMFCs to less than 1000 h of operation, and mostly, to less than 300 h (see e.g. Ref. [11] and references within). This severe limitation in cell life time currently represents the major unresolved challenge in this field.

The low performance stability of AEMFCs is mainly[1] caused by the chemical degradation of the anion conducting ionomers due to the high pH environment existent during the operation of the fuel cell [16–18]. Although AEM functional groups that are stable under well hydrated alkaline conditions have been developed [19–25], several recent studies now reveal that the high pH environment of AEMFCs *combined with a low hydration level at the cathode side of the cells*, could explain most of the chemical degradation [26–28] and the decay in performance during AEMFC operation (see e.g. Refs. [11,29]). Specifically, the high pH, combined with low hydration levels (in the membrane and in the cathode catalyst layer), exposes the quaternary ammonium (QA) cation functional groups in the ionomer to chemical attack by poorly solvated and thus highly reactive hydroxide anions [27]. This break down of the ionomeric materials in the cell leads to a continuous (and harmful) reduction of its ion exchange capacity (IEC) which, in turn, results in a continuous reduction in ionic conductivity and an increase in cell resistance, resulting in a rapid decrease in performance, as shown in the experimental literature (see e.g. Ref. [11]).

The low hydration levels encountered in the cathode, which are a result of water consumption *via* the ORR, are further reduced with increasing AEMFC current density [30]. Although the research community nowadays recognizes this phenomenon [31,32], the severity of its outcome is usually underrated, partially due to the relatively low current densities achieved in most relevant computational studies (typically smaller than 500 mA cm^{-2}) [31–37]. A recent model, which was validated at large current densities, was used to predict hydration levels in a cell simulated to operate at current densities of 1.0 A cm^{-2} and above [30]. Low levels of the hydration number ($\lambda < 10$) were found to exist in the cathode when the AEMFC was simulated to operate at low current densities, while at high values of the current density (1.0 and 2.0 A cm^{-2}), hydration number levels were respectively reduced to $\lambda = 4$ and $\lambda = 2$. Note that these calculations involved a model cell with a thin AEM (10 μm); cells with thicker AEMs are therefore expected to exhibit even lower hydration number values [31]. Finally, it is important to emphasize the correspondence between the low cathode hydration number values simulated in our previous work [30] and those ($\lambda \leq 4$) for which very fast ionomer degradation rates were observed in experimental stability tests [26].

As indicated above, most published modeling studies of AEMFCs identify the issue of low hydration levels in the cathode. However, the newly obtained understanding that these low λ values may be associated with crucially enhanced ionomer degradation has not yet been introduced into relevant models; to the best of our understanding, there are currently no models able to predict performance stability of an AEMFC. In this manuscript, we present a computational analysis of the performance of a representative AEMFC that takes into account the ionomeric material degradation and its relationship with local hydration, which depends on cell material properties, design parameters and operating cell conditions.

Our analysis is based on the introduction of degradation kinetics into an improved version of the model described in our previous study [30], where the modifications to the model as well as properties and parameters employed here are described in Section 2. Following this, in Section 3, we present results which are mainly concerned with the performance stability of representative AEMFCs as a function of two important operating and design parameters – the current density and membrane thickness. A brief summary of these results as well as the conclusions drawn from them are provided in Section 4.

2. Mathematical model and computational approach

As stated above, our approach involves the application of an updated version of our recently reported model [30], with the critical addition of ionomer degradation kinetics as a function of the local hydration of the cell. This is necessary for the prediction of realistic time-dependent deterioration of AEMFC performance. In addition, we report on an improvement of the model involving a more rigorous treatment of the gas diffusion layers (GDLs). We next provide a concise overview of our approach with an emphasis on its newer aspects; unless stated otherwise, the nomenclature remains the same as in our previous study [30] where any additional terms are explicitly defined below.

The main model equations are provided in Table 1, with boundary conditions summarized in Table 2. Modifications related to GDL modeling are included in Tables 1 and 2, while details of the newly introduced degradation kinetics are described as follows.

Modeling degradation kinetics is based on degradation data, as a function of hydration level, recently provided in the literature [26,29] for the case of the commonly used trimethylbenzyl quaternary ammonium (TMBA) functional group. Data is also available for triethylbenzyl quaternary ammonium (TEBA) but its inferior stability renders it unattractive for our current study. In fact, to the best of our knowledge, TMBA and TEBA are the only functional groups whose degradation kinetics have been measured under low hydration conditions, and TMBA is the most stable cationic group so far reported at such (low hydration) conditions (see e.g. Refs. [26,29]). Thus, TMBA is the natural choice for a representative quantitative modeling study on functional group kinetic degradation and its impact on AEMFC performance.

We assume first order kinetics according to which the ion exchange capacity (IEC), represented by the concentration of hydroxide ions (or of quaternary ammonium, due to electro-neutrality) in the ionomer (c_{OH^-}), changes with time as dictated by

$$\frac{\partial c_{OH^-}}{\partial t} = -k(\lambda, T)c_{OH^-}, \tag{1}$$

where k(λ, T) is the degradation rate constant, λ is the local hydration number ($\lambda \equiv c_{H_2O}/c_{OH^-}$.) in the cell and T is the temperature. The dependence of the rate constant on the hydration number and on temperature is extracted from experimental analyses reported in Refs. [19,26,29] with a best fit for the TMBA functional group degradation data given by

$$k(\lambda, T) = \frac{A}{1 + \alpha\lambda}\{1 - \tanh[w(\lambda - \lambda_0)]\}e^{-\frac{E_a}{RT}} \tag{2}$$

Here A, α, λ_0, w, E_a are material specific parameters provided in Table 3 (together with other properties and parameters applied in our calculations[2]). The dependence on temperature is described by the activation energy which is taken from Marino-Kreuer experimental tests [19] while the dependence on water content is fitted from experimental data reported by Dekel et al. [26,29]; this fitting is described in Fig. 1. As can be seen, two regions can be distinguished – a low hydration region characterized by a high degradation rate, and a high hydration region characterized by high functional group stability; the transition between the two regions takes place near $\lambda = \lambda_0 = 6$.

[1] Additional degradation mechanisms, worthy of investigation, exist (e.g. catalyst agglomeration). However the focus here is on the main problem which is associated with chemical attack on the ionomeric material.

[2] Unless mentioned otherwise (in Table 3, in the figure captions or in the text), properties and parameters match those used in our previous study [30].

Table 1
Main model equations.

Description	Equation
Relation between fluxes and gradients of gas phase species concentrations in the GDLs	$-\frac{c_t^g}{\varepsilon_{GDL}}\frac{\partial y_i}{\partial z}=\sum_{j,i\neq j}\frac{y_jJ_i^g-y_iJ_j^g}{\tau^{-2}D_{ij}^g}$
Relation between gas phase (mass averaged) velocity and total concentration in GDL (Darcy's law for ideal gas)	$v=-\frac{B_0R}{\mu}\frac{\partial(Tc_t^g)}{\partial z},\ B_0=\frac{d_p^2}{32}$
Equation of change of gas phase species concentrations in GDLs	$\frac{\partial c_i^g}{\partial t}=-\frac{\partial(\varepsilon_{GDL}J_i^g)}{\partial z}-\frac{\partial(c_i^gv)}{\partial z}$
Relation between diffusive molar fluxes of all gas phase species (defined with respect to mass averaged velocity)	$\sum_i Mw_iJ_i^g=0$
Relation between fluxes and gradients of gas phase species concentrations in the anode and cathode catalytic layers (CLs)	$-\frac{\partial}{\partial z}\left(\frac{c_t^g}{\varepsilon_g}\right)=\sum_{j,j\neq i}\frac{y_jN_i^g-y_iN_j^g}{\tau^{-2}D_{ij}^g}+\frac{N_i^g}{\tau^{-2}D_{iM}^g}$
Equation of change of gas phase species concentrations in anode and cathode CLs	$\frac{\partial c_i^g}{\partial t}=-\frac{\partial}{\partial z}(\varepsilon_gN_i^g)+(\delta_{iO}+\delta_{iH})R_i+\delta_{iw}E_w^g$
Relation between fluxes and gradients of concentration of water absorbed within the ionomer (in the membrane as well as in the anode and cathode CLs)	$N_w^p=-\tilde{D}_w\frac{\partial}{\partial z}\left(\frac{c_w}{\varepsilon^p}\right)-\frac{\Theta_ei_e}{F},\varepsilon^p=\frac{c_{OH^-}^p}{IEC_m},\tilde{D}_w\equiv\tau^{-2}\left(\frac{1-x_w}{D_{wOH^-}}+\frac{1}{D_{wM}}\right)^{-1},\Theta_w\equiv\frac{1-x_w}{D_{wOH^-}}\left(\frac{x_w}{D_{wOH^-}}+\frac{1}{D_{OH^-M}}\right)^{-1}$
Equations of change of free water concentration in CLs[a]	$\frac{\partial c_w^l}{\partial t}=\frac{\partial}{\partial z}\left[\varepsilon^pD_w^l\frac{\partial(c_w^l/\varepsilon^p)}{\partial z}\right]+A_w-E_w+R_w^p$
Electrolyte potential equation in membrane as well as in anode and cathode CLs	$0=\frac{\partial}{\partial z}\left(\sigma\frac{\partial\phi}{\partial z}-\Theta_wFN_w^p\right)+j$
Butler-Volmer kinetics as applied for current generation in anode and cathode CLs	$j=j_0f(c_i)a_v\left\{\exp\left[\frac{(1-\beta)nF\eta}{RT}\right]-\exp\left[-\frac{\beta nF\eta}{RT}\right]\right\}$
Overall conservation of hydroxide ions in anode and cathode CLs (balance of current generation)	$\int_{anode}\varepsilon_pR_{OH^-}^p\mathrm{d}z+\int_{cathode}\varepsilon_pR_{OH^-}^p\mathrm{d}z=0$
Rates of generation of ions in anode and cathode CLs	$R_i=-\frac{j}{F}\frac{\nu_i}{\nu_{e^-}}$

[a] Recall that, in practice, in this model free water is explicitly seen only in the anode catalytic layer.

Table 2
Boundary conditions.

Description	Expression
GDL external boundary	$c_i^g\vert_{GDL}=c_{i0}^g$
GDL/CL boundaries (gas phase species)	$c_i^g\vert_{GDL}=c_i^g\vert_{CL}$
GDL/CL boundaries (water absorbed in ionomer)	$\frac{\partial c_w}{\partial z}\vert_{CL}=0$
GDL/CL boundaries (liquid (free) water)	$c_w^l\vert_{CL}=0$
GDL/CL boundaries (electrolyte potential)	$\frac{\partial\phi}{\partial z}\vert_{CL}=0$
CL/membrane boundaries (gas phase species)	$\frac{\partial c_i^g}{\partial z}\vert_{CL}=0$
CL/membrane boundaries	$\lambda\vert_{CL}=\lambda\vert_{membrane}$

3. Results and discussion

The performance of the previous version of this model system was extensively analyzed in our earlier publication [30], in particular under a large range of current density values. However, in this previous analysis the ionomer was assumed to be perfectly stable so that, barring failure primarily due to water-management issues (e.g. drying of cathode at high current densities), simulated AEMFC operation was observed to reach a well-defined sustainable steady state.

The calculations presented in this manuscript, in which ionomer degradation is accounted for, are aimed at examining the time dependent performance of our model system for different parameter values. This can be viewed as a sensitivity analysis or, alternatively, as an attempt to identify conditions or necessary future research directions

Table 3
Properties and parameters.

Description	Expression/values
Thickness of different fuel cell layers	$w_{GDL}=190\mu m,\ w_m=28\mu m,\ w_a=5\mu m,\ w_c=5\mu m$
Gas flow channel operation conditions	$P_a=3.5atm,\ RH_a=100\%,\ P_c=3.5atm,\ RH_c=90\%$
GDL porosity	$\varepsilon_{GDL}=0.\ 8$
CL gas transport porosities	$\varepsilon_g=\varepsilon_s-(c_w+c_w^l)V_m,\ \varepsilon_s=0.\ 29,\ \tau=1$
Molecular and Knudsen gas diffusion coefficients	Defined by Gilliland and Knudsen equations for corresponding gases. See Ref. [30]
GDL pore diameter	$d_p=\ 10\mu m$. See Ref. [38]
Ionomer/air humidification equilibrium [39]	$\lambda_{RH}=26.\ 66RH^3-28.\ 6RH^2+13.\ 14RH-0.\ 158$
Anode and cathode catalyst layer structure	Carbon volume = 36.5%, Catalyst volume = 3.7%, Ionomer loading = 0.16 mg cm^{-2}
Water diffusivity in ionomer as a function of λ and IEC (equal to c_{OH^-}) (fitted from data provided in Ref. [1]). Units of hydroxide concentration – mole/liter.	$\tilde{D}_w(c_{OH^-},\lambda)=1.\ 66{\cdot}10^{-11}\lambda\times Exp\{1.\ 3[c_{OH^-}(x,t)-c_{OH^-}(x,0)]\}\ m^2sec^{-1}$
Polymer tortuosity within catalytic layers	$\tau^p=2.2$
Hydroxide conductivity in ionomer as a function of λ and IEC (equal to c_{OH^-}) (fitted from data provided in Ref. [1]). Units of hydroxide concentration – mole/liter. $\lambda_{max}=12$.	$\sigma(c_{OH^-},\lambda)=0.\ 5(0.\ 78\lambda^4\lambda_{max}^{-3}+0.\ 22\lambda)\times Exp\{1.\ 3[c_{OH^-}(x,t)-c_{OH^-}(x,0)]\}\ mScm^{-1}$
Degradation kinetics parameters	$A=3.\ 14{\cdot}10^{17}\frac{1}{s},\ \alpha=5.\ 799,\ E_a=1.\ 33{\cdot}10^5\ J/mole,\ w=6,\ \lambda_0=6$

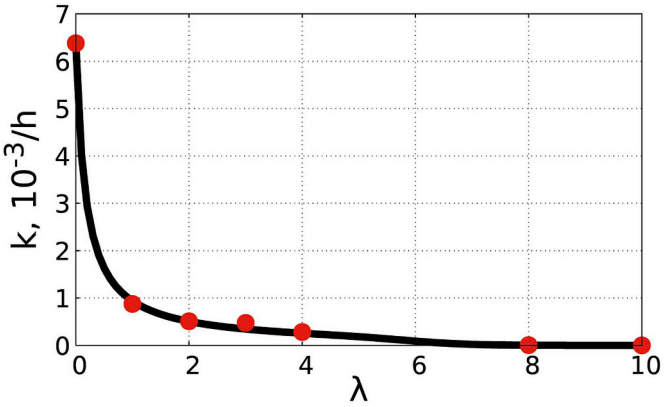

Fig. 1. Experimental (red circles – from Refs. [26,29]) and fitted (black continuous line) degradation kinetic coefficient of the TMBA functional group as a function of the hydration number λ at T= 22°C. (For interpretation of the references to colour in this figure legend, the reader is referred to the Web version of this article.)

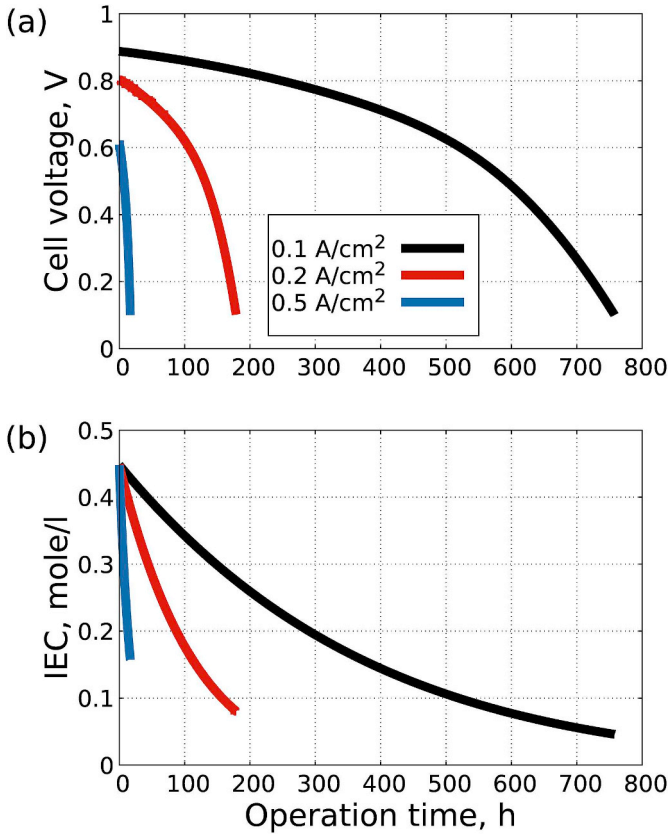

Fig. 2. (a) Simulated cell performance stability of an AEMFC operated at different current densities; (b) simulated average IEC of the ionomer in the cathode (moles of functional group per unit total volume of material in the cathode) during the same cell operation time. (For interpretation of the references to colour in this figure legend, the reader is referred to the Web version of this article.)

leading to sustainable high-performance of AEMFCs, at least for time-periods long enough to be of practical value (for instance, for automotive applications). To this end, we start by examining the impact of current density on cell longevity. In Fig. 2a we present the predicted change in performance over time of an AEMFC operated at constant current density values of 0.1, 0.2 and 0.5 A cm^{-2}. As can be seen, performance stability decreases significantly with time, and in all cases, the cell is rendered practically useless after less than 800 h. This is

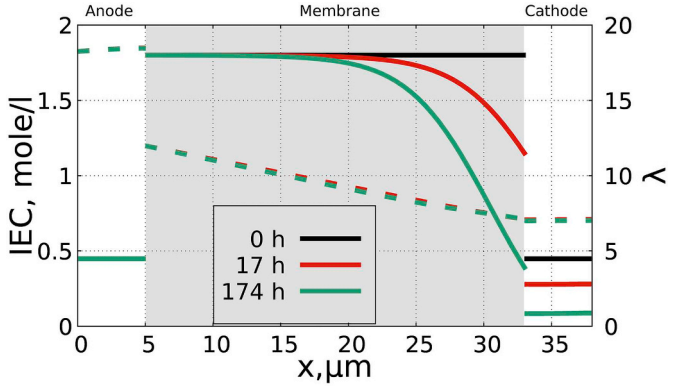

Fig. 3. Ion exchange capacity (IEC) (full lines) and hydration number (λ) (dashed lines) across the cell, at the initial stage (t = 0 h) as well as at 17 h and 174 h after onset of AEMFC operation. The (constant) current density is 0.2 A cm^{-2} and the thickness of the AEM is 28 μm. (For interpretation of the references to colour in this figure legend, the reader is referred to the Web version of this article.)

consistent with previous experimental studies where reported life time of AEMFCs are below 800 h (see e.g. Ref. [11]), and is directly associated with continuous chemical degradation of the ionomer [27,29]. This is clearly apparent when looking at Fig. 2b which depicts the spatially averaged IEC of the ionomer in the cathode, calculated during the same simulations considered in Fig. 2a. Notice how the reduction of ionomer IEC with time (due to its degradation), seen in Fig. 2b, is indeed correlated with the deterioration of performance (shown in Fig. 2a), and both grow in importance with increasing current density. From a mechanistic point of view, during AEMFC operation time, the reduction in IEC decreases the anion conductivity of the ionomer, which in turn causes decay in performance, as seen in Fig. 2a.

It is known that the rate of degradation is related to the degree of hydration [26,29]. Indeed, this was incorporated into our kinetic model as discussed in the previous section. As shown in previous calculations [30], the level of hydration is highly non-uniform across the cell; this is primarily due to the fact that, during AEMFC operation, water is produced in the anode and consumed in the cathode. Therefore, we expect the rate of degradation, and the resultant time-dependent IEC *distribution*, to reflect this non-uniformity in hydration. Simulated local IEC profiles across the anion conducting polymer (AEM and ionomers within the catalyst layers) are shown in Fig. 3 for a constant current density of 0.2 A cm^{-2} (corresponding to the red curves in Fig. 2). These profiles, obtained at three different cell operation times (0, 17 and 174 h), clearly reflect the impact of local hydration values (also shown in Fig. 3) on degradation. Prior to cell operation, IEC levels are equal to the imposed initial uniform values (1.8 and 0.45 mol l^{-1} for the AEM and ionomer in the catalyst layers, respectively). After onset of cell operation, the IEC profile in the membrane becomes non uniform, exhibiting increasingly reduced values with increasing time and distance from the anode/membrane interface. At the same time, the IEC profile in the cathode, although nominally uniform, continuously drops as cell operation time progresses while the IEC profile in the anode remains unchanged. This behavior can be easily understood when considering the spatial distribution of water content in the membrane and catalyst layers. As already mentioned above, discussed in our previous study [30] and clearly seen in Fig. 3, hydration number values λ at any given time during cell operation, significantly decrease from the anode across the membrane to the cathode. This non-uniform λ profile causes the rate of degradation to be non-uniform *via* the dependence of the degradation kinetic coefficient on λ (see Fig. 1 and Eq. (2)). Thus, as seen in Fig. 3, degradation is most pronounced in the driest regions of the cell, i.e. the cathode (also quantified in Fig. 2b) as well as regions of the membrane adjacent to the cathode. This process does not affect the IEC of the anode side, as this electrode is saturated in water, a condition at

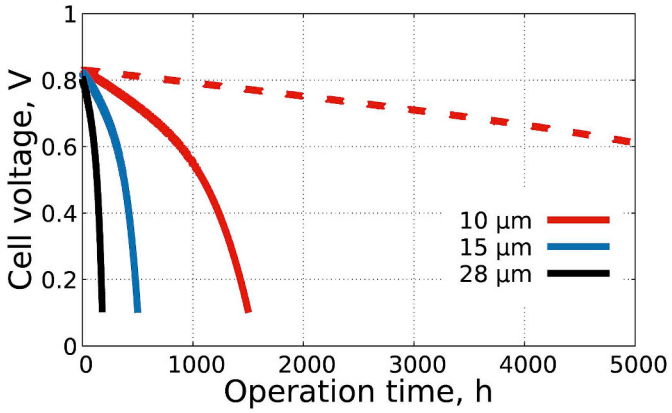

Fig. 4. Simulated cell performance stability of AEMFCs operated at a constant current density of 0.2 A cm^{-2} and with different AEM thickness values (10 μm, 15 μm and 28 μm). Full lines were calculated with kinetic parameters given in Table 3. The dashed red line (10 μm AEM) was calculated with the same kinetic parameters except for "A" which in this case is reduced by a factor of 5 ($A = 6.28 \cdot 10^{16} \frac{1}{s}$). (For interpretation of the references to colour in this figure legend, the reader is referred to the Web version of this article.)

which the ionomeric material is chemically stable [29].

From a quantitative point of view, in an AEMFC operated at a current density of 0.2 A cm^{-2}, the IEC of the AEM *at the interface with the cathode* (seen in Fig. 3) degrades from 1.8 mol l^{-1} to around 1.2 mol l^{-1} and 0.4 mol l^{-1} after 17 and 174 h of operation, respectively. Similarly, the IEC *in the cathode* (seen in Fig. 3) degrades from 0.45 mol l^{-1} to around 0.28 mol l^{-1} and 0.09 mol l^{-1} after 17 and 174 h of operation, respectively. This significant reduction in IEC well explains the significant reduction in AEMFC performance during time, as shown in Fig. 2a.

Looking again at Fig. 2a, we next focus on the sensitivity of performance reduction to current density. The reason for the decrease in longevity with increasing current density values is directly related to the hydration of the cathode side of the cell. It has been reported that, at higher current densities, water gradients across the cell are more pronounced and lower hydration numbers are obtained at the cathode side [30]. Also, both theoretical and experimental studies report that at $\lambda < 4$ functional groups are more rapidly degraded [26,40]. With the increased degradation rate of functional groups (primarily in the cathode and cathode-side of the membrane) at increased current densities, the IEC decreases more rapidly, leading to a faster deterioration in AEMFC performance at higher current densities as shown in Fig. 2a.

The reduction in the IEC (shown in Fig. 2b) is caused by the dry-out of the cathode during operation of the cell, as can be observed (for the case of 0.2 A cm^{-2}) in Fig. 3. If the thickness of the AEM is reduced below 28 μm, the resultant enhanced water transport from anode to cathode may enable an increase in the cathode hydration number value, thereby creating an environment less favorable for ionomer degradation. This is investigated *via* calculations whose results are depicted in Fig. 4; these show the effect of AEM thickness on the simulated performance stability of an AEMFC operated under a constant current density of 0.2 A cm^{-2}. It can be clearly observed that as AEM thickness is reduced, AEMFC performance stability significantly increases. For instance, cell life-time increases from around 180 h to 500 and almost 1500 h when AEM thickness is reduced from 28 μm to 15 and 10 μm, respectively.

The promotion of AEMFC stability, *via* the reduction in AEM thickness (see Fig. 4), is a simple way to improve stability. Another seemingly obvious option, involves using functional groups with increased stability properties. Here we quantitatively test this option by assuming we have a hypothetical new functional group whose chemical degradation kinetic parameter "A" (see Eq. (2) and Table 3) is five times smaller than that measured with TMBA [26] and used in all of the calculations discussed thus far (see Fig. 1 and Table 3).[3] Performance stability of an AEMFC using this hypothetical functional group is shown in Fig. 3 for a 10 μm thick AEM (dashed red line). Application of this AEM, results in a simulated AEMFC life-time significantly above 5000 h, which matches the fuel cell life-time DOE 2020's requirement for automotive applications [41]. The theoretical ability to achieve such an impressive cell life-time, by tuning two parameters (AEM thickness and degradation kinetics of the ionomeric materials) provides critical insight on materials requirements that will lead to highly stable AEMFC tests.

4. Conclusions

We have developed a unique model capable of predicting AEMFC performance stability *in operando*. The model takes into account the degradation of ionomeric materials and their dependence on the local hydration levels, which are in turn related to the cell material properties, design parameters and cell operating conditions. The model demonstrates, for the first time in the literature of AEMFCs, the strong impact of operating current density and membrane characteristics on cell performance stability and life-time. The predicted cell performance stability, which is based on representative materials, design and operating parameters for AEMFCs, is short and consistent (in a semi-quantitative manner) with AEMFC stability data reported in the literature ([11,42–44]). However, by using thinner membranes and improved materials with reduced degradation kinetics (k = 0.0256 1/h for $\lambda = 4$ and T = 60 °C), the model predicts a substantial improvement in the stability; an AEMFC life-time significantly higher than 5000 h is theoretically achieved, satisfying the DOE 2020's cell life-time target for automotive applications.

We believe that, although based on representative materials, design and operating parameters, this study and its results provide important ideas and targets for near-future materials design, crucial for the development of viable AEMFC technology. Future availability of degradation data (under realistic operating conditions), of additional promising ionomer material systems, should make it possible to apply our model for quantitatively more accurate stability predictions for systems other than the representative cell considered here.

Acknowledgment

The authors wish to thank Noga Ziv from the Nancy & Stephan Grand Technion Energy Program (GTEP) and Karam Yassin from the Wolfson Department of Chemical Engineering at the Technion for their help with the preparation of the final form of the manuscript. This work was partially funded by the Nancy & Stephan Grand Technion Energy Program (GTEP); by the European Union's Horizon 2020 research and innovation program [grant No. 721065]; by the Ministry of Science, Technology and Space of Israel through the Israel-Germany Batteries Collaboration Call 2017 [German grant No. 2675], and through grant No. 3-12948; by the Israel Science Foundation [grant No. 1481/17]; by the Russell Berrie Nanotechnology Institute, Technion; by the Israel Innovation Authority through the KAMIN program [grant No. 60503]; and by the Ministry of National Infrastructure, Energy and Water Resources of Israel [grant No. 3-13671]. The authors would also like to acknowledge the financial support of Melvyn & Carolyn Miller Fund for Innovation, as well as the support of Planning & Budgeting Committee/ ISRAEL Council for Higher Education and Fuel Choice Initiative (Prime Minister Office of ISRAEL), within the framework of "Israel National Research Center for Electrochemical Propulsion (INREP)".

[3] At the operating temperature assumed here (60 °C), for a hydration number value of $\lambda = 4$, the factor of five reduction in the parameter "A" translates to a reduction in the (first order) kinetic coefficient "k" value from 0.128 h^{-1} to 0.0256 h^{-1}.

References

[1] S. Gottesfeld, D.R. Dekel, M. Page, C. Bae, Y. Yan, P. Zelenay, Y.S. Kim, Anion exchange membrane fuel cells: current status and remaining challenges, J. Power Sources 375 (2018) 170–184, https://doi.org/10.1016/j.jpowsour.2017.08.010.

[2] H.A. Miller, A. Lavacchi, F. Vizza, M. Marelli, F. Di Benedetto, F. D'Acapito, Y. Paska, M. Page, D.R. Dekel, A Pd/C-CeO 2 anode catalyst for high-performance platinum-free anion exchange membrane fuel cells, Angew. Chem. 128 (2016) 6108–6111, https://doi.org/10.1002/ange.201600647.

[3] H.A. Miller, F. Vizza, M. Marelli, A. Zadick, L. Dubau, M. Chatenet, S. Geiger, S. Cherevko, H. Doan, R.K. Pavlicek, S. Mukerjee, D.R. Dekel, Highly active nanostructured palladium-ceria electrocatalysts for the hydrogen oxidation reaction in alkaline medium, Nanomater. Energy 33 (2017) 293–305, https://doi.org/10.1016/j.nanoen.2017.01.051.

[4] E.S. Davydova, S. Mukerjee, F. Jaouen, D.R. Dekel, Electrocatalysts for hydrogen oxidation reaction in alkaline electrolytes, ACS Catal. 8 (2018) 6665–6690, https://doi.org/10.1021/acscatal.8b00689.

[5] M. Bellini, H.A. Miller, M. Pagliaro, F. Vizza, A. Lenarda, P. Fornasiero, M. Marelli, C. Evangelisti, Q. Jia, S. Mukrejee, J. Jankovic, L. Wang, J. Varcoe, C. Sharma, I. Grinberg, E. Davydova, D.R. Dekel, Palladium-ceria catalysts with enhanced alkaline hydrogen oxidation activity for anion exchange membrane fuel cells, Appl. Energy Mater. (2019) (submitted, under review).

[6] S. Kabir, K. Lemire, K. Artyushkova, A. Roy, M. Odgaard, D. Schlueter, A. Oshchepkov, A. Bonnefont, E. Savinova, D.C. Sabarirajan, P. Mandal, E.J. Crumlin, I.V.V. Zenyuk, P. Atanassov, A. Serov, Platinum group metal-free NiMo hydrogen oxidation catalysts: high performance and durability in alkaline exchange membrane fuel cells, J. Mater. Chem. A. 5 (2017) 24433–24443, https://doi.org/10.1039/c7ta08718g.

[7] Q. Hu, G. Li, J. Pan, L. Tan, J. Lu, L. Zhuang, Alkaline polymer electrolyte fuel cell with Ni-based anode and Co-based cathode, Int. J. Hydrog. Energy 38 (2013) 16264–16268, https://doi.org/10.1016/j.ijhydene.2013.09.125.

[8] D.R. Dekel, Alkaline membrane fuel cell (AMFC) materials and system improvement - state-of-the-art, ECS Trans. 50 (2013) 2051–2052, https://doi.org/10.1149/05002.2051ecst.

[9] M. Alesker, M. Page, M. Shviro, Y. Paska, G. Gershinsky, D.R. Dekel, D. Zitoun, Palladium/nickel bifunctional electrocatalyst for hydrogen oxidation reaction in alkaline membrane fuel cell, J. Power Sources 304 (2016) 332–339, https://doi.org/10.1016/j.jpowsour.2015.11.026.

[10] J.R. Varcoe, P. Atanassov, D.R. Dekel, A.M. Herring, M.A. Hickner, P.A. Kohl, A.R. Kucernak, W.E. Mustain, K. Nijmeijer, K. Scott, T. Xu, L. Zhuang, Anion-exchange membranes in electrochemical energy systems, Energy Environ. Sci. 7 (2014) 3135–3191, https://doi.org/10.1039/C4EE01303D.

[11] D.R. Dekel, Review of cell performance in anion exchange membrane fuel cells, J. Power Sources 375 (2018) 158–169, https://doi.org/10.1016/j.jpowsour.2017.07.117.

[12] T.J. Omasta, L. Wang, X. Peng, C.A. Lewis, J.R. Varcoe, W.E. Mustain, Importance of balancing membrane and electrode water in anion exchange membrane fuel cells, J. Power Sources 375 (2018) 205–213, https://doi.org/10.1016/j.jpowsour.2017.05.006.

[13] L. Wang, E. Magliocca, E.L. Cunningham, W.E. Mustain, S.D. Poynton, R. Escudero-Cid, M.M. Nasef, J. Ponce-González, R. Bance-Souahli, R.C.T.T. Slade, D.K. Wheligan, J.R. Varcoe, An optimised synthesis of high performance radiation-grafted anion-exchange membranes, Green Chem. 19 (2017) 831–843, https://doi.org/10.1039/C6GC02526A.

[14] L. Wang, M. Bellini, H.A. Miller, J.R. Varcoe, A high conductivity ultrathin anion-exchange membrane with 500+ h alkali stability for use in alkaline membrane fuel cells that can achieve 2 W cm-2at 80 °c, J. Mater. Chem. A. 6 (2018) 15404–15412, https://doi.org/10.1039/c8ta04783a.

[15] T.J. Omasta, X. Peng, H.A. Miller, F. Vizza, L. Wang, J.R. Varcoe, D.R. Dekel, W.E. Mustain, Beyond 1.0 W cm −2 performance without platinum: the beginning of a new era in anion exchange membrane fuel cells, J. Electrochem. Soc. 165 (2018) J3039–J3044, https://doi.org/10.1149/2.0071815jes.

[16] A.D. Mohanty, C. Bae, Mechanistic analysis of ammonium cation stability for alkaline exchange membrane fuel cells, J. Mater. Chem. A. 2 (2014) 17314–17320, https://doi.org/10.1039/c4ta03300k.

[17] M.R. Sturgeon, C.S. Macomber, C. Engtrakul, H. Long, B.S. Pivovar, Hydroxide based benzyltrimethylammonium degradation: quantification of rates and degradation technique development, J. Electrochem. Soc. 162 (2015) F366–F372, https://doi.org/10.1149/2.0271504jes.

[18] A.D. Mohanty, S.E. Tignor, M.R. Sturgeon, H. Long, B.S. Pivovar, C. Bae, Thermochemical stability study of alkyl-tethered quaternary ammonium cations for anion exchange membrane fuel cells, J. Electrochem. Soc. 164 (2017) F1279–F1285, https://doi.org/10.1149/2.0141713jes.

[19] M.G. Marino, K.D. Kreuer, Alkaline stability of quaternary ammonium cations for alkaline fuel cell membranes and ionic liquids, ChemSusChem 8 (2015) 513–523, https://doi.org/10.1002/cssc.201403022.

[20] A.G. Wright, J. Fan, B. Britton, T. Weissbach, H.-F. Lee, E.A. Kitching, T.J. Peckham, S. Holdcroft, Hexamethyl-p-terphenyl poly(benzimidazolium): a universal hydroxide-conducting polymer for energy conversion devices, Energy Environ. Sci. 9 (2016) 2130–2142, https://doi.org/10.1039/C6EE00656F.

[21] K.M. Hugar, H.A. Kostalik, G.W. Coates, Imidazolium cations with exceptional alkaline stability: a systematic study of structure-stability relationships, J. Am. Chem. Soc. 137 (2015) 8730–8737, https://doi.org/10.1021/jacs.5b02879.

[22] S.A. Nuñez, C. Capparelli, M.A. Hickner, N-alkyl interstitial spacers and terminal pendants influence the alkaline stability of tetraalkylammonium cations for anion exchange membrane fuel cells, Chem. Mater. 28 (2016) 2589–2598, https://doi.org/10.1021/acs.chemmater.5b04767.

[23] H.-S.S. Dang, P. Jannasch, Anion-exchange membranes with polycationic alkyl side chains attached: via spacer units, J. Mater. Chem. A. 4 (2016) 17138–17153, https://doi.org/10.1039/c6ta05939b.

[24] J. Fan, A.G. Wright, B. Britton, T. Weissbach, T.J.G. Skalski, J. Ward, T.J. Peckham, S. Holdcroft, Cationic polyelectrolytes, stable in 10 M KOH aq at 100 °C, ACS Macro Lett. 6 (2017) 1089–1093, https://doi.org/10.1021/acsmacrolett.7b00679.

[25] A.D. Mohanty, C.Y. Ryu, Y.S. Kim, C. Bae, Stable elastomeric anion exchange membranes based on quaternary ammonium-tethered polystyrene- b -poly(ethylene- co -butylene)- b -polystyrene triblock copolymers, Macromolecules 48 (2015) 7085–7095, https://doi.org/10.1021/acs.macromol.5b01382.

[26] D.R. Dekel, M. Amar, S. Willdorf, M. Kosa, S. Dhara, C.E. Diesendruck, Effect of water on the stability of quaternary ammonium groups for anion exchange membrane fuel cell applications, Chem. Mater. 29 (2017) 4425–4431, https://doi.org/10.1021/acs.chemmater.7b00958.

[27] C.E. Diesendruck, D.R. Dekel, Water – a key parameter in the stability of anion exchange membrane fuel cells, Curr. Opin. Electrochem. 9 (2018) 173–178, https://doi.org/10.1016/j.coelec.2018.03.019.

[28] S. Willdorf-Cohen, A.N. Mondal, D.R. Dekel, C.E. Diesendruck, Chemical stability of poly(phenylene oxide)-based ionomers in an anion exchange-membrane fuel cell environment, J. Mater. Chem. A. 6 (2018) 22234–22239, https://doi.org/10.1039/C8TA05785K.

[29] D.R. Dekel, S. Willdorf, U. Ash, M. Amar, S. Pusara, S. Dhara, S. Srebnik, C.E. Diesendruck, The critical relation between chemical stability of cations and water in anion exchange membrane fuel cells environment, J. Power Sources 375 (2018) 351–360, https://doi.org/10.1016/j.jpowsour.2017.08.026.

[30] D.R. Dekel, I.G. Rasin, M. Page, S. Brandon, Steady state and transient simulation of anion exchange membrane fuel cells, J. Power Sources 375 (2018) 191–204, https://doi.org/10.1016/j.jpowsour.2017.07.012.

[31] K. Jiao, P. He, Q. Du, Y. Yin, Three-dimensional multiphase modeling of alkaline anion exchange membrane fuel cell, Int. J. Hydrog. Energy 39 (2014) 5981–5995, https://doi.org/10.1016/j.ijhydene.2014.01.180.

[32] Y.-J. Sohn, J.-I. Choi, K. Kim, Numerical analysis on water transport in alkaline anion exchange membrane fuel cells, Electrochemistry 83 (2015) 80–83, https://doi.org/10.5796/electrochemistry.83.80.

[33] K. Jiao, S. Huo, M. Zu, D. Jiao, J. Chen, Q. Du, An analytical model for hydrogen alkaline anion exchange membrane fuel cell, Int. J. Hydrog. Energy 40 (2015) 3300–3312, https://doi.org/10.1016/j.ijhydene.2014.12.091.

[34] H.S. Shiau, I.V. Zenyuk, A.Z. Weber, Water management in an alkaline-exchange-membrane fuel cell, ECS Trans. 69 (2015) 985–994, https://doi.org/10.1149/06917.0985ecst.

[35] S. Peng, J. Gong, X. Xu, P.C. Sui, S. Lu, Y. Xiang, Numerical and experimental analyses on deviated concentration loss with alkaline anion-exchange membrane fuel cells, J. Phys. Chem. C 119 (2015) 24276–24281, https://doi.org/10.1021/acs.jpcc.5b08031.

[36] H. Deng, D. Wang, X. Xie, Y. Zhou, Y. Yin, Q. Du, K. Jiao, Modeling of hydrogen alkaline membrane fuel cell with interfacial effect and water management optimization, Renew. Energy 91 (2016) 166–177, https://doi.org/10.1016/j.renene.2016.01.054.

[37] B.S. Machado, N. Chakraborty, P.K. Das, Influences of flow direction, temperature and relative humidity on the performance of a representative anion exchange membrane fuel cell: a computational analysis, Int. J. Hydrog. Energy 42 (2017) 6310–6323, https://doi.org/10.1016/j.ijhydene.2016.12.003.

[38] M. Bosomoiu, G. Tsotridis, T. Bednarek, Study of effective transport properties of fresh and aged gas diffusion layers, J. Power Sources 285 (2015) 568–579, https://doi.org/10.1016/j.jpowsour.2015.03.132.

[39] Q. Duan, S. Ge, C.-Y.Y. Wang, Water uptake, ionic conductivity and swelling properties of anion-exchange membrane, J. Power Sources 243 (2013) 773–778, https://doi.org/10.1016/j.jpowsour.2013.06.095.

[40] S. Pusara, S. Srebnik, D.R. Dekel, Molecular simulation of quaternary ammonium solutions at low hydration levels, J. Phys. Chem. C 122 (2018) 11204–11213, https://doi.org/10.1021/acs.jpcc.8b00752.

[41] DOE Technical Targets for Fuel Cell Systems and Stacks for Transportation Applications, (n.d.). https://www.energy.gov/eere/fuelcells/doe-technical-targets-fuel-cell-systems-and-stacks-transportation-applications.

[42] B. Pivovar, Advanced Ionomers & MEAs for Alkaline Membrane Fuel Cells, DOE Hydrogen and Fuel Cells Program 2018 Annual Merit Review and Peer Evaluation Meeting, https://www.hydrogen.energy.gov/pdfs/review18/fc147_pivovar_2018_o.pdf.

[43] S. Maurya, S. Noh, I. Matanovic, E.J. Park, C.N. Villarrubia, U. Martinez, J. Han, C. Bae, Y.S. Kim, Rational design of polyaromatic ionomers for alkaline membrane fuel cells with > 1 W cm^{-2} power density, Energy Environ. Sci. 11 (2018) 3283–3291, https://doi.org/10.1039/c8ee02192a.

[44] X. Peng, T.J. Omasta, E. Magliocca, L. Wang, J.R. Varcoe, W.E. Mustain, Nitrogen-doped carbon–CoO_x nanohybrids: a precious metal free cathode that exceeds 1.0 wcm^{-2} peak power and 100 h life in anion-exchange membrane fuel cells, Angew. Chem. Int. Ed. 57 (2018) 1–7, https://doi.org/10.1002/anie.201811099.

Journal of Membrane Science 586 (2019) 140–150

Contents lists available at ScienceDirect

Journal of Membrane Science

journal homepage: www.elsevier.com/locate/memsci

Effect of CO_2 on the properties of anion exchange membranes for fuel cell applications

Noga Ziv[a,b], Abhishek N. Mondal[a], Thomas Weissbach[c], Steven Holdcroft[c], Dario R. Dekel[a,b,*]

[a] The Wolfson Department of Chemical Engineering, Technion – Israel Institute of Technology, Haifa, 3200003, Israel
[b] The Nancy & Stephan Grand Technion Energy Program (GTEP), Technion – Israel Institute of Technology, Haifa, 3200003, Israel
[c] Department of Chemistry, Simon Fraser University, 8888 University Drive, Burnaby, BC, V5A 1S6, Canada

ARTICLE INFO

Keywords:
Anion exchange membranes
Fuel cells
CO_2
Carbonation
Ionic conductivity

ABSTRACT

In this study the effect of CO_2, HCO_3^- and CO_3^{2-} on the ionic conductivity and water uptake properties of anion exchange membranes (AEMs) was investigated in order to better understand the detrimental effect of ambient air feed on the performance of AEM fuel cells. Three types of AEMs were examined, including Poly(hexamethyl-*p*-terphenyl benzimidazolium) (HMT-PMBI), Fumatech® FAA-3, and poly(phenylene oxide) functionalized with imidazole (PPO-Im). The effect of temperature and humidity on AEM properties in their different anion forms was studied, including both steady state and dynamic measurements. In addition, the response to changes in CO_2 concentration and to application of ex-situ electric current was examined. Results showed that an increase in humidity leads to an increase in water content and an increase in conductivity of the AEMs, regardless the anion type. It was found that both temperature and relative humidity improve conductivity in carbonated forms, however relative humidity has the most significant impact. The carbonation process in 400 ppm CO_2 is slightly quicker in AEMs with low conductivity, lasting ca. 40 min; however it was shown that a reverse process can be achieved by applying an electric current through the AEMs. An increase by 2–10 fold in conductivity is obtained using this method, which is analogous to the changes observed during operation of the fuel cell. This work provides important data that needs to be taken into account in future work in order to ultimately mitigate the carbonation effects and improve the performance of AEM fuel cells running with ambient air.

1. Introduction

Anion exchange membrane fuel cells (AEMFCs) have recently gained much attention as highly effective, clean energy devices, since they offer significant advantages over the presently common proton exchange membrane fuel cells (PEMFCs) [1]. These advantages include the ability to use lower cost non-platinum group metals as catalysts [2–10], lower H_2 fuel crossover, and in addition the absence of KOH aqueous electrolyte (as opposed to previous alkaline fuel cells - AFCs) impedes the precipitation of carbonate salts [11] and stabilizes the catalyst layer [12]. In spite of these significant advantages, for the AEMFC technology to become widely accepted, a few challenges still need to be overcome – among them, increasing the chemical stability of the anion exchange membranes [13–20], developing highly active electrocatalysts towards the hydrogen oxidation reaction [21] and decreasing the negative effect of CO_2 on the AEM properties, are probably the most important ones that needs to be currently addressed.

The latter challenge is critical in order to allow AEMFCs to operate with ambient air. When ambient air is used to run a cell, OH^- anions that are created in the oxygen reduction reaction (Equation (1)) react with CO_2 from the air and produce bulkier and less mobile CO_3^{2-} and HCO_3^- anions (Equation (2) and (3)) [22].

$$O_2 + 2H_2O + 4e^- \rightarrow 4OH^- \quad (1)$$

$$OH^- + CO_2 \rightarrow HCO_3^- \quad (2)$$

$$HCO_3^- + OH^- \rightarrow CO_3^{2-} + H_2O \quad (3)$$

In a comprehensive review on the effect of CO_2 on AEMFCs, Ziv et al. [22] showed that peak power density and voltage of AEMFCs using CO_2-free gas was almost twice higher than that of a fuel cell operating with ambient air (~400 ppm CO_2) [6,18,23–25]. This is most likely due to the lower CO_3^{2-} and HCO_3^- conductivity compared to OH^- conductivity of AEMs; measurements of CO_3^{2-} and HCO_3^- conductivity in literature range between 2 and 10 times lower than OH^- [22]. The lower values stem from the lower ionic mobility of CO_3^{2-} and HCO_3^-, which is related to the larger ionic radius and mass of these

* Corresponding author. The Wolfson Department of Chemical Engineering, Technion – Israel Institute of Technology, Haifa, 3200003, Israel.
E-mail address: dario@technion.ac.il (D.R. Dekel).

https://doi.org/10.1016/j.memsci.2019.05.053
Received 30 March 2019; Received in revised form 20 May 2019; Accepted 21 May 2019
Available online 24 May 2019
0376-7388/

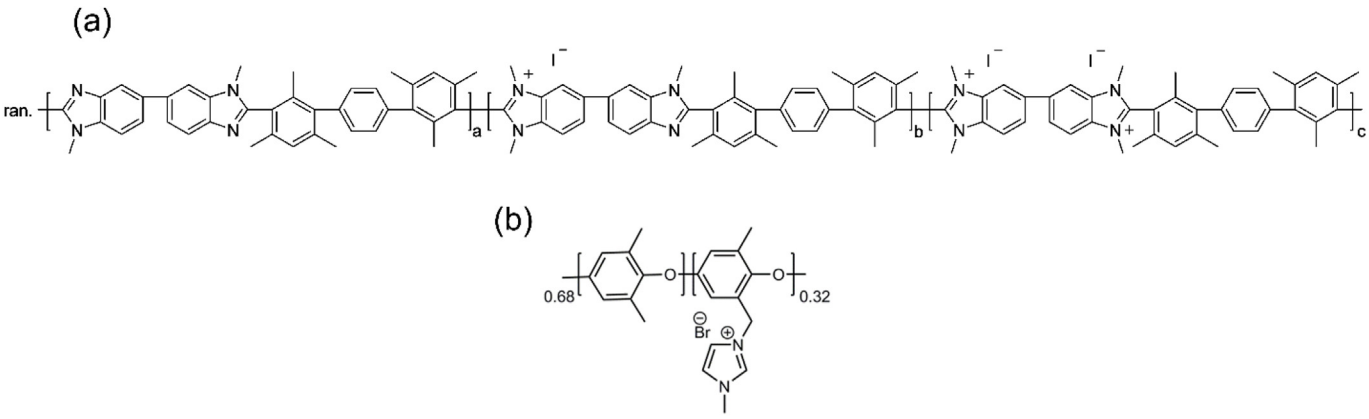

Fig. 1. Chemical Structure of the AEMs (a) HMT-PMBI and (b) PPO-Im (FAA-3 is a commercial AEM and its exact structure is unknown).

anions (the hydration radii for solvated OH^-, CO_3^{2-}, and HCO_3^- in an aqueous solution have been reported as 3, 3.94 [26], and 5.6 Å [27], respectively). Reduction in anion conductivity occurs also due to the lower degree of dissociation of carbonate anions from the membrane's functional groups [28,29], which means that less anions are free to move through the membrane. In addition, OH^- anions have access to the Grotthus (proton hopping) transport mechanism, as opposed to CO_3^{2-} and HCO_3^- which rely on diffusion and convection alone [30,31].

While CO_3^{2-} and HCO_3^- have a detrimental effect on the membrane's conductivity, it was found that they can increase the AEM chemical stability compared to the case of OH^-, since carbonate anions are weaker nucleophiles than hydroxide anion [32]. This could suggest that operating with ambient air could reduce the membrane degradation seen in AEMFC longevity tests. However, it has been reported that CO_3^{2-} and HCO_3^- concentration in the AEM decreases during operation under high current densities due to a so-called carbonate self-purging mechanism [25,33–35]. This phenomenon occurs at increasing current densities due to the high rate of OH^- production in the cathode, which surpasses the rate of CO_2 absorption from the ambient air. Nevertheless, according to a recent numerical model describing the carbonation effects on operation of an AEMFC [36], it was shown that even at relatively high current densities, the AEM contains a mixture of OH^-, CO_3^{2-} and HCO_3^- anions. Therefore, the study of AEM properties in these three anion forms is critical to understand the effect of CO_2 on the membrane and on the AEMFC during its operation on ambient air.

The effect of using ambient air on AEMFC performance was investigated only in 3% of literature reports [37]. So far, only very few studies have dealt with the effect CO_2 has on key AEM properties that affect AEMFC performance, such as water uptake and conductivity [38–42]. Recently, Peng et al. [38], Pandey et al. [40] and Suzuki et al. [41] studied the effect of OH^-, CO_3^{2-} and HCO_3^- anions on water uptake, conductivity and water transport properties of A201 AEMs (Tokuyama, Japan) [38,41] and Fumasep® FAA-3 AEMs (Fumatech, Germany) [40]. In addition, Divekar et al. studied the carbonation process kinetics in perfluorinated-based AEMs by transient SAXS measurements [39], and the effect of temperature and CO_2 concentration on equilibrium anion composition in the AEM [42]. Even though these studies are important to the understanding of the effect of CO_2 on AEMs, they did not consider the transient behavior of carbonated AEMs under changing ambient conditions, which is relevant in fuel cell applications. In addition, it is important to study the CO_2 effect in diverse AEM types and structures and to investigate the influence of ambient conditions on this effect.

In this work we present a new study on the impact of the carbonate species anions on the conductivity and water uptake properties of a highly conductive AEM (HMT-PMBI), and its comparison with an AEM with similar functional group in a different polymeric backbone as well as comparison with the commercially available FAA-3 AEM from Fumatech (Germany). Also, for the first time non steady-state behavior is reported of carbonates in the AEMs. Results may significantly contribute to the knowledge and understanding of AEM behavior during operation of AEMFCs under ambient air.

2. Experimental

2.1. Materials

PPO [poly(2,6-dimethyl-1,4-phenylene oxide)] was obtained from Sigma Aldrich, AIBN (α,α -Azoisobutyronitrile) was obtained from Glentham Life Sciences, 1-Methylimidazole and NBS (*N*-bromosuccinimide) were purchased from Alfa Aesar, chloroform was purchased from Merck, ethanol 96% was purchased from Gadot, NMP (n-Methyl-2-pyrrolidone) was purchased from Carlo Erba reagents, and chlorobenzene was purchased from Fisher Scientific. Ion-exchange solutions were prepared using A.R. purity KOH, $KHCO_3$ and K_2CO_3, purchased from Spectrum Chemical MFG corp.

2.2. Anion exchange membranes

HMT-PMBI AEM – AEM composed of 2,2″,4,4″,6,6″-hexamethyl-*p*-terphenylene (HMT) and *N*-methylated poly(benzimidazolium)s (PMBI), with an 89.3% degree of methylation was prepared, as described in detail elsewhere [43]. The cationic functional groups in this membrane are part of the polymer backbone rather than tethered along the backbone as in PPO-based AEMs (see Fig. 1a). The HMT-PMBI film was prepared via casting from DMSO at 80 °C, soaked in H_2O for 24 h, and dried under vacuum at 80 °C [44]. The AEM was reported to have IEC of 2.5 mmol/g and thickness of ca. 50 μm [44].

Synthesis of 1-Methylimidazole functionalized PPO – The procedure to prepare brominated PPO (Br-PPO) is described below. 12 g PPO (100 mmol) was vigorously stirred in chlorobenzene (100 mL) till it completely dissolved. Afterwards, 8.9 g (50 mmol) of NBS was added in parts to the previously stirred PPO solution. To start the reaction AIBN (2,2′-azobis-isobutyronitrile, 0.5 g, 3 mmol) was added as a free radical initiator to the reaction mixture. To ensure the progress of the reaction, the entire mixture was heated under reflux conditions (135 °C) for 3 h. After cooling the solution, a 10-fold excess of ethanol was used to precipitate the product. The obtained polymer was successively filtered and washed several times with ethanol, and then re-dissolved in chloroform (110 mL). The polymer solution was precipitated into a 10-fold excess of ethanol solution. The desired polymer was obtained as a white powder and dried under vacuum for overnight to get Br-PPO with a degree of bromination of 32% (DS = 0.32), which is confirmed by ^1H NMR spectroscopy. To prepare 1-Methylimidazole functionalized PPO, firstly, a 25 mL round bottom flask was charged with 10 mL NMP

solution. Afterwards, a known amount of Br-PPO (1.0 g) prepared in the previous step was slowly added to the stirred NMP solution till complete dissolution. In the follow up step, a suitable quantity of 1-Methylimidazole (0.217 g) was introduced inside the reaction mixture in a dropwise manner. To ensure the complete reaction between brominated PPO and 1-Methylimidazole, the reaction temperature was raised to 50 °C and stirred further for additional 24 h. Finally, the polymer solution was casted on top of a clean glass plate and dried at ambient temperature (60 °C) for 24 h to obtain a transparent light brown thin film. The final synthesized membrane is designated as PPO-Im (see chemical structure in Fig. 1b). The ion exchange capacity (IEC) of the AEM was measured by Mohr titration (described elsewhere [45]) and found to be 1.64 mmol/g.

Fumatech® FAA-3 AEMs – This AEM (referred to as FAA-3) was purchased from Fumatech BWT GmbH (Germany). The general chemistry of this AEM is not disclosed. The AEM's IEC is between 1.5 and 1.8 mmol/g and thickness between 25 and 35 μm [46].

While HMT-PMBI contains imidazolium groups in the polymer backbone, PPO-Im contains imidazolium as pendant groups which allows some exploration of the effect of the cationic group's location on the AEM properties. FAA-3 is a benchmark AEM which serves as a comparison source for both AEMs.

2.3. Anion exchange process

To obtain AEMs in their HCO_3^- form and CO_3^{2-} form, the membranes were immersed in 1 M $KHCO_3$ and K_2CO_3 (Spectrum Chemical MFG corp.), respectively, for 48 h, followed by immersion in DI water (> 18MΩ) for 48 h (with frequent change of DI water). To obtain OH^- form AEMs, the membrane samples were immersed in 1 M KOH inside a glovebox under inert nitrogen atmosphere containing less than 10 ppm CO_2 (limit of detection) for 48 h. Subsequently, the samples were rinsed in degassed DI water (dissolved CO_2 was removed prior to use) inside the glovebox to remove residual KOH. Solutions of different carbonate concentrations were prepared from mixtures of KOH and K_2CO_3 so that the total anion concentration is 1 M ($[CO_3^{2-}] + [OH^-] = 1$ M). HCO_3^- cannot exist in these solutions since the composition is determined by several equilibrium constants simultaneously, so that either OH^- and CO_3^{2-} coexist in the solution, or CO_3^{2-} and HCO_3^-.

2.4. Anion conductivity

After the corresponding ion-exchange process, AEMs (sized 1 cm × 3 cm) in their HCO_3^- and CO_3^{2-} form were mounted in the conductivity measurement cell and inserted into the measurement chamber of a MTS-740 (Membrane Test System) supplied by Scribner Inc. (USA). AEMs in their OH^- form were mounted in the cell inside the N_2-filled glovebox and then quickly moved into the sealed measurement chamber under continuous Ar stream. Conductivity was calculated using the membrane resistance (R, Ω) measured in a sealed, insulated chamber under continuous pure N_2 gas flow. The membrane samples were equilibrated at 40 °C and different relative humidity (RH) steps. RH was swept from 90% to 50% (desorption), then back to 90% (adsorption) in 10% intervals. The membrane samples were first equilibrated at 90% RH for 1 h and then at each of the RH steps for 45 min. The two directions of conductivity measurements are presented in Fig. 2.

Through-plane resistance was measured as previously reported [47], using a 4-probe method with 2 current collecting and 2 potential sensing platinum electrodes. A PSM1735 Frequency Response Analyzer (Newtons4th Ltd) with AC potential amplitude of 10 mV and frequency range of 10^7–1 Hz was utilized, and the ionic resistance was extracted as the real-axis high frequency intercept. Through-plane (TP) conductivity value was then calculated as:

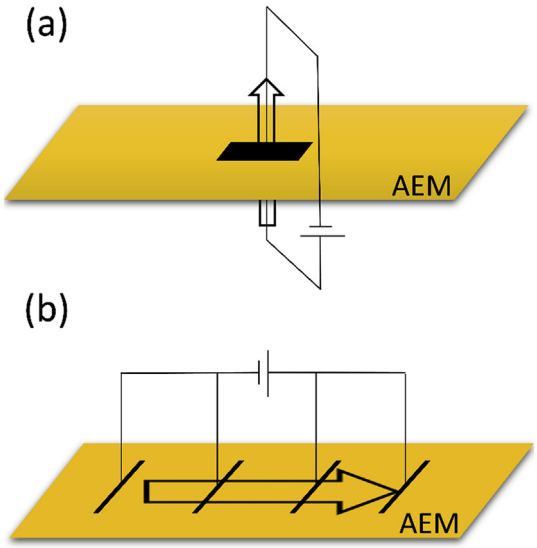

Fig. 2. Schematic representation of (a) through-plane (TP) and (b) in-plane (IP) directions of the membrane.

$$\sigma_{TP} = \frac{d}{A \cdot R} \tag{4}$$

where d (cm) is the membrane thickness, A is the overlapping area of the current collecting electrodes (constant at 0.5 cm^2) and R (Ω) is the measured resistance.

In-plane resistance was measured in a 4 platinum electrode cell (BT-110, BekkTech, LLC) by performing a linear voltage sweep [47] using SP-300 Potentiostat (Bio-Logic). The ionic resistance is extracted as the slope of voltage vs. current and the in-plane (IP) conductivity value is then calculated as:

$$\sigma_{IP} = \frac{L}{d \cdot W \cdot R} \tag{5}$$

where L is the distance between the sense electrodes (constant at 0.425 cm), d (cm) is the thickness of the membrane, W (cm) is the width of the membrane sample and R (Ω) is the measured resistance.

2.5. Dynamic conductivity measurements

The AEM anion conductivity during the carbonation and CO_2 self-purging process was measured using a novel technique recently reported for measuring the true hydroxide conductivity [48]. In this technique a direct electric current is applied in the in-plane direction of an AEM which initially contains HCO_3^- anions. In the first stage, HCO_3^--form AEM is equilibrated at 40 °C and 90% RH until a stable conductivity value is measured. Then, a constant current of 100 μA is applied through the AEM, with brief interruptions every 10–30 min to measure the ionic conductivity (using cyclic voltammetry). The conductivity is monitored until the value is stabilized, at which point the true OH^- conductivity of the AEM is measured.

2.6. Water uptake

The water uptake (WU) of the AEMs was measured using TA Instruments' VTI-SA + (USA). The membrane samples were equilibrated with hydrated N_2 flow (according to the desired RH value). RH steps started from 90% to 50% (desorption) followed by increase back to 90% (adsorption), with 10% incremental steps. At each RH step, the samples were allowed to reach equilibrium (until a change of less than 0.001% in weight was recorded). Water uptake was then calculated as:

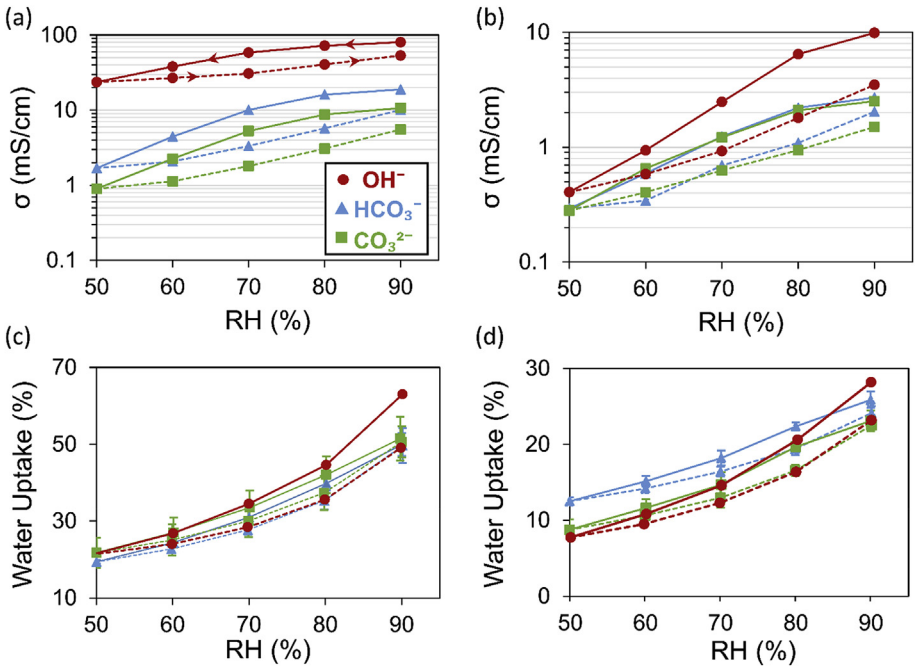

Fig. 3. Through-plane conductivity of HMT-PMBI (a) and FAA-3 (b) and water uptake of HMT-PMBI (c) and FAA-3 (d) as a function of relative humidity during desorption (solid line) and adsorption (dashed line) in different anion forms at 40 °C: OH^- (●), HCO_3^- (▲) and CO_3^{2-} (■).

$$WU\ [\%] = \frac{W_{(RH)} - W_{dry}}{W_{dry}} \cdot 100\% \quad (6)$$

where $W_{(RH)}$ is the weight of the membrane after equilibration in the RH step and W_{dry} is the weight of the dry membrane (measured using a microbalance after drying the sample in a vacuum oven at 40 °C overnight).

3. Results and discussion

3.1. Characterization of AEM properties in OH^-, HCO_3^- and CO_3^{2-} forms

One of the main factors impacting the movement of anions through the membrane is the level of hydration, affecting the disassociation of anions from the cationic groups [49]. Fig. 3a and b shows the effect of the ambient RH on the measured OH^-, HCO_3^- and CO_3^{2-} through-plane conductivity of HMT-PMBI and FAA-3 AEMs, respectively. As mentioned previously, OH^- conductivity is significantly higher in both AEM types: HMT-PMBI OH^- conductivity is between 6 and 10 times higher than HCO_3^- and CO_3^{2-} conductivity, reaching up to 80 mS/cm which is in agreement with values reported in literature [43,50,51]. The higher conductivity especially in low RH could mean that OH^- form membranes can adsorb water better than HCO_3^- and CO_3^{2-}. FAA-3 OH^- conductivity is almost 5 times higher than HCO_3^- and CO_3^{2-} at 90% RH, but only 1.3 times higher at 50% RH, implying that in this membrane hydration affects more greatly on OH^- conductivity. The ratios of OH^- to HCO_3^-/CO_3^{2-} conductivity in high RH are in agreement with most ratios found in literature which fall between 4 and 8 [22,38–40]. HCO_3^- and CO_3^{2-} conductivities in both AEMs are relatively similar, even though CO_3^{2-} is a divalent anion and has a smaller hydration radius compared to HCO_3^-. Since the number of cationic groups in the AEM is fixed (for a given IEC), in order to maintain charge neutrality, the concentration of CO_3^{2-} in the AEM is half of that of HCO_3^-, affecting then the anion conductivity measured in the AEMs in this anion form.

As expected, the increase in RH leads to a significant increase in conductivity of both AEMs regardless the anion type. Anion conductivity in all forms is 10–25 times higher in high humidity (90% RH) compared to low humidity (50% RH), confirming that high RH is necessary in order to achieve better AEMFC performance and performance stability when it operates with ambient air [52].

The differences in conductivity values can be explained by the differences in the water uptake of the membranes, as it was found that OH^-, HCO_3^- and CO_3^{2-} have different (increasing) hydration shells [28], affecting the water uptake of the membranes in their different anion forms. This effect can be seen in HMT-PMBI and FAA-3 in Fig. 3c and d, respectively. For example, HMT-PMBI shows 26% higher water uptake in OH^- form than CO_3^{2-} form at 90% RH, which may account for some of the higher OH^- anion conductivity. Similar conclusions were reached by Divekar et al. [39], who measured a decrease in the AEM water uptake during exposure to ambient air corresponding to the decrease in OH^- concentration. Also, Marino et al. [53] and Peng et al. [38] measured higher water uptake in OH^- form AEM corresponding to higher anion conductivity.

Another factor affecting the anion conductivity is the membrane structure; HMT-PMBI shows between 3 and 50 times higher conductivity than FAA-3, which can be partially explained by the lower water uptake in FAA-3 AEM but may also relate to morphological differences between the membranes. Morphology studies of the HMT-PMBI AEM show that these materials contain no phase separation or water clustering on small length scales and no characteristic length scales at all above the monomer length, which is uncommon among high-performance fuel cell membranes [54]. In addition, it was recently found that HMT-PMBI shows higher water permeation than FAA-3 both from liquid and from gas phase [55], which accounts for part of its higher water uptake presented here.

An interesting phenomenon observed in both anion conductivity and water uptake is the hysteresis during desorption (decreasing RHs) and adsorption (increasing RHs). When the membrane is losing water to the environment (desorption), its water uptake in equilibrium is higher than when it is adsorbing water (adsorption) from the environment, at the same RH conditions [45,56]. This is likely due to strong bonds between the water molecules inside the membrane, and bonds between water and anions/functional groups [45]. This hysteresis phenomenon was previously observed in other water absorbing polymers [57] and was linked to changes in the polymer morphology; as water leaves the voids between polymer chains become smaller, and the volume available for water decreases. This may be of great importance during AEMFC operation, where changes in relative water contents and/or water content gradients through the membrane occur when dynamic

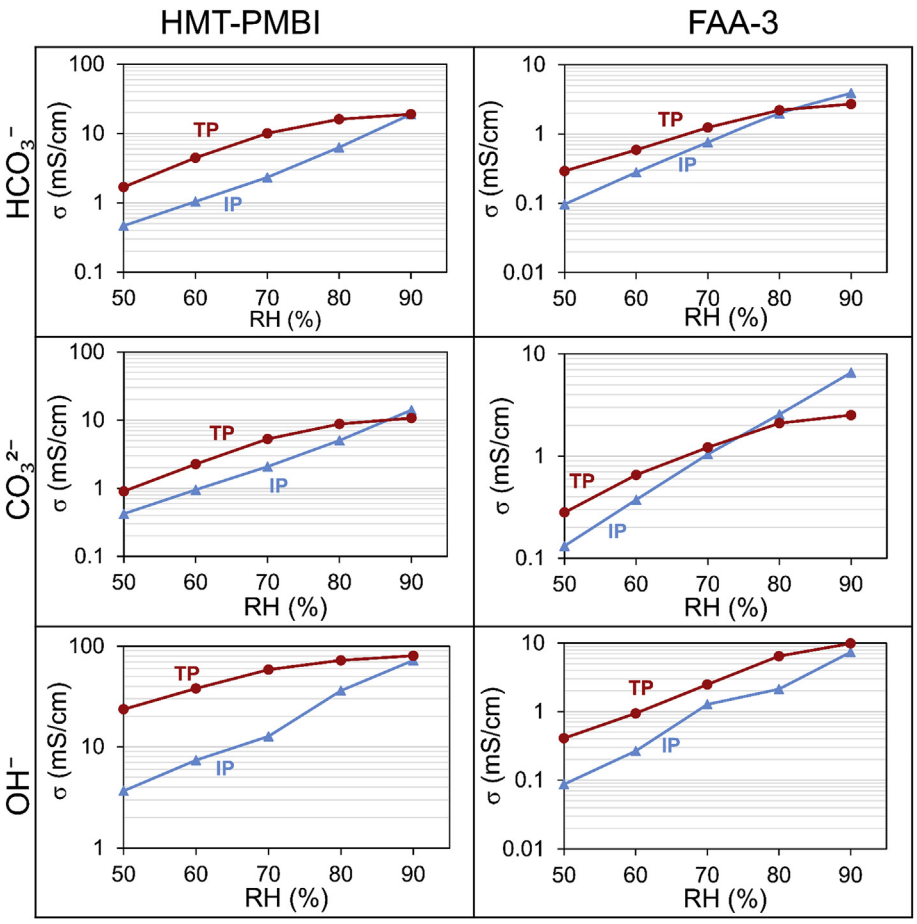

Fig. 4. Through-plane (●) and in-plane (▲) conductivity at 40 °C of HCO_3^- (top), CO_3^{2-} (middle) and OH^- (bottom) anions in HMT-PMBI (left) and FAA-3 (right) AEMs.

operating conditions are applied to the cell.

Through-plane (TP) conductivity values are important as they are most representative of the direction of anion transport during AEMFC operation. However, the most commonly measured conductivity in literature is the in-plane (IP) conductivity, which is easier to measure.

To study the effect of direction of measurement on the conductivity, Fig. 4 compares the anion conductivity of two AEMs (HMT-PMBI and FAA-3) for IP and TP directions in OH^-, HCO_3^-, and CO_3^{2-} anions. As expected, both IP and TP anion conductivities increase with increasing RH, however, it is visible that in both AEMs, IP conductivity is significantly lower than TP at low RH values. At 50% RH for instance, the IP conductivity of HCO_3^-, CO_3^{2-} and OH^- anions is about 3, 12 and 6 times lower than TP conductivity, respectively. This can be explained by the harsher effect that low humidity has on the anion transport on the surface layers of the membrane compared to the effect on the bulk [45,58]. As water leaves the membrane at low RH, the surface layers are drier than the bulk and therefore the anion mobility in these layers is lower. At high RH, the surface layers and the bulk are fully hydrated and the difference between TP and IP conductivity is minimal.

In addition to the above, Fig. 4 again shows the considerably higher OH^- conductivity than carbonate (HCO_3^- and CO_3^{2-}) conductivity in both AEMs and both IP and TP directions.

Since the anions' diffusion coefficients in the AEM depend strongly on temperature [49], increasing the operating temperature can lead to a significant increase in the anion conductivity of the membrane. Fig. 5a presents the TP conductivity of HMT-PMBI AEM as a function of RH at 40 °C and 60 °C. As expected, conductivity values are higher at 60 °C for all the anions [59]; however, the ratio of OH^- conductivity to HCO_3^- conductivity is slightly lower at higher temperatures. The OH^-/HCO_3^- conductivity ratio is ~4 at 40 °C (80 mS/cm and 20 mS/cm for OH^- and HCO_3^-, respectively) compared to 3 at 60 °C (90 mS/cm and 30 mS/cm

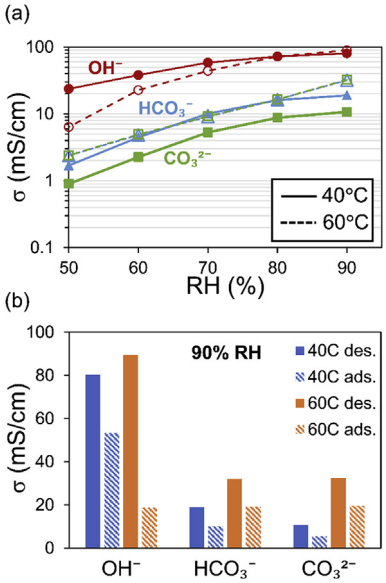

Fig. 5. (a) Through-plane conductivity of HMT-PMBI at 40 °C and 60 °C as a function of RH, and (b) a comparison between conductivity values during desorption and adsorption at 90% RH.

for OH^- and HCO_3^- respectively). A possible reason could be lower water uptake of OH^- form AEM at higher temperature, as observed by Divekar et al. [39], which could influence the anion conductivity. The reduction in conductivity ratio could suggest that an AEMFC working at higher temperatures could mitigate the decrease in cell performance as a result of carbonation. This was also previously discussed in the

context of lower CO_2 solubility in higher temperature, which leads to a lower degree of carbonation [36,60]. However, Krewer et al. [36] theoretically showed that higher temperature increases HCO_3^- and CO_3^{2-} concentration in the AEM, and in addition Divekar et al. [42] did not measure a significant difference in OH^- concentration at higher temperature, so the effect of temperature on carbonation in an AEMFC in operation is still inconclusive, and further studies are needed to clarify this effect.

Furthermore, there is a significant decrease in OH^- conductivity during the adsorption process (RH increase), clearly visible in Fig. 5b. We attribute this decrease in conductivity to the accelerated degradation process of the HMT-PMBI AEM in its OH^- form while exposed to low hydration levels at higher temperatures [14]. However, it was previously reported that HMT-PMBI does not go through chemical degradation in high OH^- concentration for ca. 100 h, but rather some morphological reorganization which affects the conductivity [43]. This conductivity decrease is not so severe in the AEMs in the case of HCO_3^- and CO_3^{2-} anions, as in this case the anions are less nucleophilic than OH^- and therefore the AEMs are more stable [22,32].

Other than ambient conditions and measurement configuration, the cationic functional groups play the most important role in the binding and transport of anions through the membrane [1]. The cation position inside the polymer may affect the spatial arrangement of the polymer chains in the membrane and therefore its properties, such as stability, water uptake and anion transport.

As previously described, the structure of HMT-PMBI membranes is based on linear polymer chains containing imidazolium cationic groups as part of the backbone [43,44]. As part of this work, a second AEM was synthesized (PPO-Im), based on a PPO backbone functionalized with imidazolium pendant groups, of similar characteristics to the imidazolium cation of the HMT-PMBI AEM. Fig. 6a shows conductivity properties of PPO-Im (HMT-PMBI is shown in Fig. 3a). We recognize that the polymer backbones are different, and this plays a major role in the polymer conductivity; however, it is of interest to try and compare the effect of the position of imidazolium group inside the AEM polymer on the anion conductivity values.

As can be seen, HMT-PMBI conductivity is significantly higher than PPO-Im (for example, 80 mS/cm compared to 19 mS/cm at 90% RH, 40 °C). This may stem from higher water uptake (displayed in Fig. 6b),

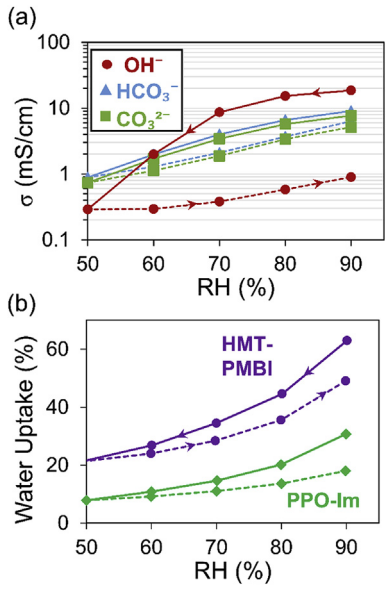

Fig. 6. (a) PPO-Im Anion TP conductivity vs. RH at 40 °C during desorption (solid line) and adsorption (dashed line) in OH^- (●), HCO_3^- (▲) and CO_3^{2-} (■) forms; (b) Water uptake of HMT-PMBI (●) and PPO-Im (♦) as a function of RH during desorption (solid line) and adsorption (dashed line) (at 40 °C).

but may also suggest that imidazolium incorporated in the polymer backbone can improve anion conductivity compared to imidazolium as a side group. It was previously reported that HMT-PMBI has a unique morphology, enabling water to form interpenetrating network where conductivity can be favored [54]. In addition, OH^- conductivity of PPO-Im AEM is significantly lower during adsorption, which might indicate degradation of the functional groups at lower RH [14]. In contrast, this degradation is not observed in HMT-PMBI AEMs, as in these membranes the imidazolium cationic group is sterically protected in the backbone and is not prone to rapid degradation [43,44,61]. It can also be observed that the ratio of OH^- to HCO_3^-/CO_3^{2-} conductivity is between 4 and 8 in HMT-PMBI, and only 2–3 in PPO-Im. This could support the suggestion raised previously that its unique structure can encourage higher water uptake, and the water molecules' arrangement in chains between the polymer chains facilitate anion transport [54].

To conclude, anion conductivity in AEMs in equilibrium is affected by ambient conditions (such as RH and temperature), measurement configuration and AEM structure. In all cases, OH^- shows superior conductivity as compared to HCO_3^- and CO_3^{2-}. However, a decrease in RH leads to larger conductivity loss in OH^- form AEMs than in carbonate forms, meaning it has slightly higher sensitivity to low RH conditions.

3.2. Study of transient behavior of AEMs in OH^-, HCO_3^- and CO_3^{2-} forms

Fuel cells devices are usually required to have a fast response to external inputs. Therefore, it is important to study their dynamic behavior during external changes in order to optimize their performance during non-steady state steps, such as shut down, start up or changes in environments. In addition, during AEMFC operation, water is consumed in the cathode and produced in the anode, which may cause water gradients and changes in RH in the vicinity of the AEM and therefore in the membrane's hydration level (which was highlighted as critical for AEMFC performance [52,62]). This in turn, leads to changes in membrane conductivity which affect the cell performance.

Fig. 7 shows the transient anion conductivity (TP and IP) values of HMT-PMBI, FAA-3 and PPO-Im AEMs immediately after removing from wet state (fully hydrated) in room temperature to 90% RH at 40 °C, for HCO_3^-, CO_3^{2-} and OH^- anions. During this change in ambient conditions the membrane loses water to the ambient carrier gas (N_2), changing its water content and its thickness (due to swelling), which in turn affects the conductivity value. In almost all cases the conductivity increases in the first stage of the process. In some cases, the conductivity reached a maximum value followed by decrease and stabilization (for example all anions' IP conductivity) and in others it simply reaches a plateau (for example HCO_3^- TP conductivity). The maximum in the IP measurements could be a result of the following process: First, the ambient temperature increases, causing the anion mobility to increase. In the next stage, the membranes continue to lose water to the environment (as it is fully hydrated in the beginning), and therefore the conductivity decreases.

In contrast to HCO_3^- and CO_3^{2-} conductivities, OH^- conductivity, in both IP and TP directions and in all AEM types, slowly decreases after the initial stabilization; for example, TP OH^- conductivity of HMT-PMBI decreases during the period of 2.5 – 6 h by ca. 10% (from 47 mS/cm to 42 mS/cm), while HCO_3^- TP conductivity decreases by only 0.7% in the same period of time (14.5–14.4 mS/cm). The larger decrease in OH^- conductivity could be due to a slow process of carbonation by exposure to very low concentrations of CO_2, or partially due to some degree of degradation, since OH^- is much stronger nucleophile than HCO_3^- and CO_3^{2-}. It should be noted that in an operating AEMFC, OH^- anions are constantly produced in the cathode, which could affect OH^- conductivity changes in time.

It is visible from Fig. 7 that the time in which the membrane reaches a stable value is slightly shorter in TP conductivity measurements; for example, a change of less than 1% in HMT-PMBI HCO_3^- conductivity is

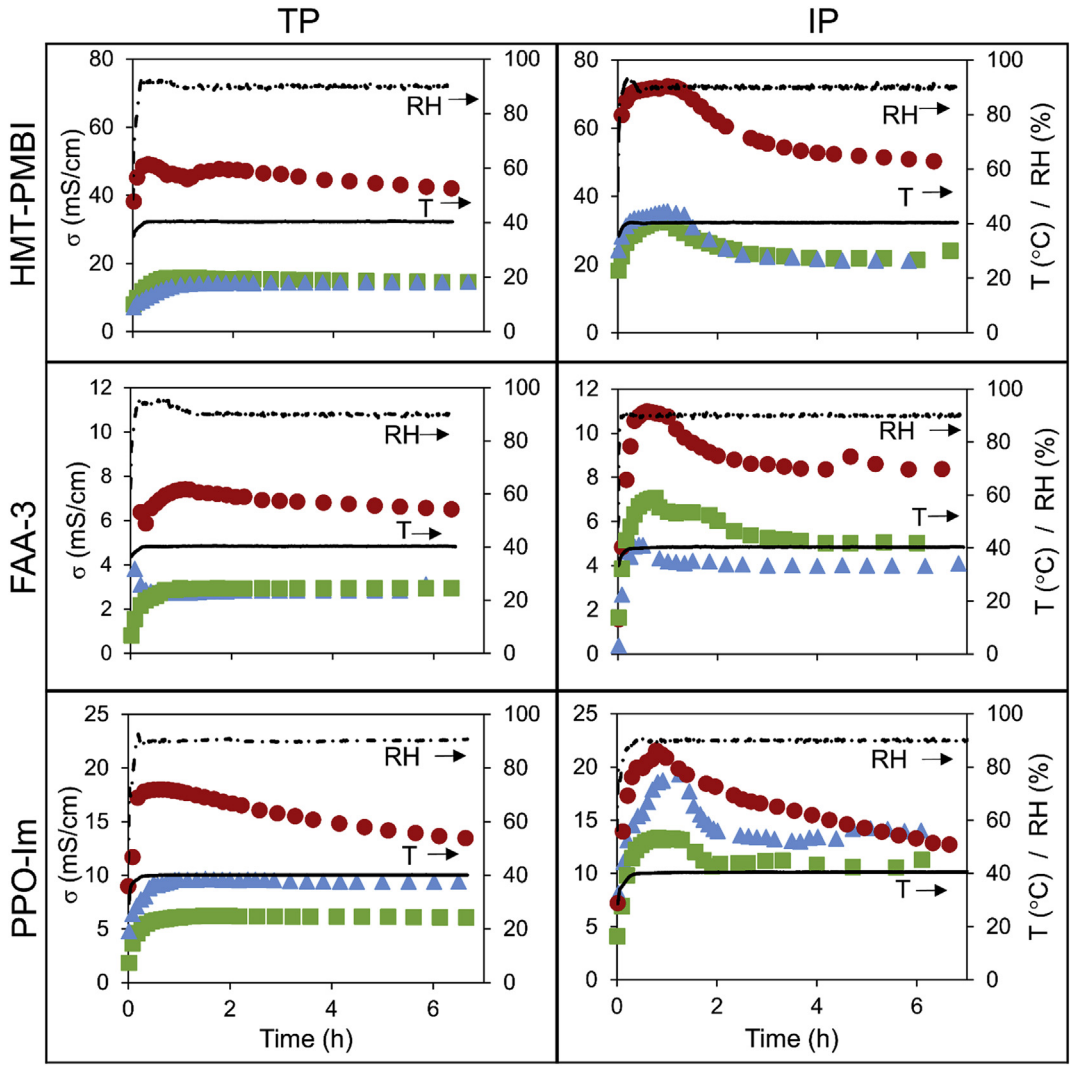

Fig. 7. Conductivity changes during transition from wet (fully hydrated) state in RT to 90% RH in 40 °C for OH^- (●), HCO_3^- (▲) and CO_3^{2-} (■). Changes in RH (dashed line) and temperature (solid line) are also displayed.

measured after 3.5 h in IP measurements and after only 2 h in TP measurements. Since water uptake from the environment should be independent of direction and therefore equal in both measurements, this could mean that TP conductivity is less sensitive to changes in RH or membrane hydration. The same idea was raised previously in Fig. 4, where IP conductivity was lower than TP at lower RH. However, the longer equilibration time could also result from the difference in measurement procedure: in TP measurements a force is applied on the membrane which partially limits the change in thickness, as opposed to IP measurements where the thickness and width of the membrane sample can freely change. In addition, TP conductivity is calculated based on thickness alone while IP is based on thickness and width, which could have affected the calculated conductivity values.

Results show that the equilibration time of HMT-PMBI AEMs is ca. 2 – 3 h, slightly longer than that the equilibration time of the FAA-3 and PPO-Im AEMs (ca. 1 – 2 h). This might suggest slower kinetics in HMT-PMBI, but the original thickness of the membrane should also be considered. HMT-PMBI thickness decreases by nearly 50% during the process due to its higher liquid water uptake while PPO-Im thickness decreases by ca. 10% and FAA-3 decreases by less than that.

Another important kinetics data is the process of absorption of CO_2 into the AEMs in their OH^- form, denominated as the carbonation process. During start up or shut down of an AEMFC, the membrane might be exposed to ambient air and CO_2 will be absorbed into the AEM [22]. The transient effect of adding 400 ppm CO_2 to the surrounding gas on the AEMs' TP conductivity was measured. The general experimental response obtained through all the three studied AEMs were similar (see Fig. 8a) – the effective anion conductivity decreases quickly immediately after changing the environment from 0 ppm to 400 ppm CO_2. HMT-PMBI conductivity stabilizes after ca. 40 min, FAA-3 after ca. 30 min and PPO-Im after ca. 60 min. In order to compare the kinetics of the carbonation process between the three AEMs, the time which is required to reach 50% of the total decrease in conductivity is calculated and presented in Fig. 8b.

These results are in agreement with similar previous measurements where carbonation of AEMs in their OH^- form was completed in a period of 15 min to 2 h [35,39,43,53,63,64]. Marino et al. [53] measured anion concentration in FAA-3 during carbonation and showed that after 30 min ca. 30% of the initial OH^- anions remains. The quicker decrease in conductivity measured here could imply that carbonate species affects AEM conductivity even in moderate concentrations, as it will be shown later in this work.

Similar results were previously achieved by theoretical calculations based on carbonation reaction kinetics and thermodynamics [65].

The differences in carbonation times between different AEMs may be explained by the differences in their IEC – while HMT-PMBI AEM has the highest IEC (2.5 mmol/g), FAA-3 and PPO-Im have ca. 1.7 mmol/g and 1.64 mmol/g, respectively, therefore the initial amount of OH^- in

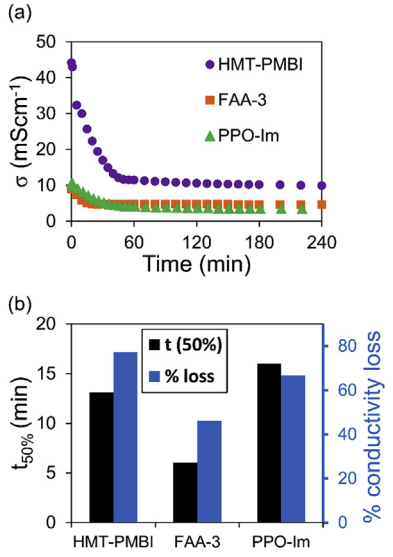

Fig. 8. (a) Kinetics of carbonation process at 40 °C for HMT-PMBI (●), FAA-3(■) and PPO-Im (▲) AEMs. t = 0 is the time of switching ambient gas from pure N_2 to N_2 + 400 ppm CO_2. (b) Characteristic time to reach 50% carbonation (black) and percent of total change in conductivity from the initial value (blue) for the different AEMs. (For interpretation of the references to colour in this figure legend, the reader is referred to the Web version of this article.)

the membrane is higher. Another aspect affecting the carbonation process is the initial conductivity value and the total change in conductivity. It can be seen in Fig. 8a that HMT-PMBI conductivity decreases by ca. 33 mS/cm (77% change) compared to only 4 mS/cm in FAA-3 (67% change), and therefore the time it takes to reach the lower value is significantly longer.

A simple numerical model was built based on the generic model described by Krewer et al. [36] on carbonation effects on AEMFCs. This simple model allows predicting the changes in anion concentration in HMT-PMBI AEM during the carbonation process. The concentrations were then used to calculate the expected conductivity at each time step according to:

$$\sigma = \sum z_i C_i \sigma_i \tag{7}$$

where z_i is the charge of species i, (i = OH^-, CO_3^{2-} and HCO_3^-), C_i is the relative ratio of species i in the AEM (predicted by the model) and σ_i is the conductivity of the AEM containing only species i (where σ_{OH} was taken as the initial measured conductivity). The results of the simulated conductivity transient values and their comparison to the experimental data (Fig. 8a) are presented in Fig. 9. According to the simplistic model, the entire initial amount of OH^- in the membrane is replaced by CO_3^{2-} and HCO_3^- anions in less than 20 min. These changes in anion concentration profiles in the AEM lead to a sharp decrease in the membrane

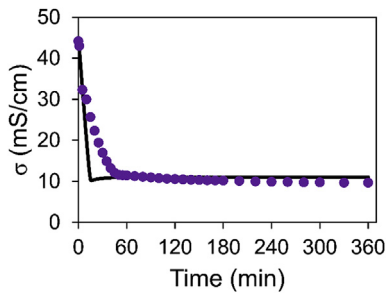

Fig. 9. Model results (solid line) and experimental results (dots) for TP conductivity during exposure of OH^--form HMT-PMBI AEM to gas containing 400 ppm CO_2 at 40 °C.

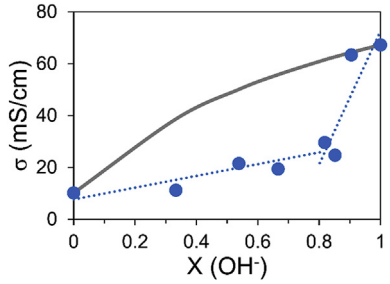

Fig. 10. HMT-PMBI through-plane conductivity at 40 °C and 90% RH as a function of the equivalent fraction of OH^- in a 1 M anion solution.

conductivity, which stabilizes at the final value after ~20 min. Experimentally, the membrane's conductivity decreases by nearly 80% and reached the final value in ca. 40 min. This is a rough estimate based on theoretical data and therefore deviations from experimental results are possible; however, this could also imply that the conductivity of the membrane does not depend linearly on anion species concentration.

During the carbonation steps, the AEM contains mixtures of OH^-, HCO_3^- and CO_3^{2-} anions in changing ratios, thus affecting the total ionic conductivity [22]. An interesting parameter is the capability of the membrane to absorb HCO_3^- and CO_3^{2-} anions from an aqueous solution and their effect on the membrane's conductivity. This was examined by preparing aqueous solutions of different CO_3^{2-} and OH^- concentrations (maintaining constant total anion concentration of 1 M) and measuring anion conductivity of an AEM which was immersed in these solutions. The fraction of OH^- ions in the solution, out of the total concentration of equivalent ion-exchanging groups, x_{OH^-}, is described in Equation (8) (CO_3^{2-} occupies two cationic sites at the same time) and the measured AEM conductivity is displayed in Fig. 10. The solid line represents the theoretical calculation assuming the ratio in the membrane is equal to the ratio in the solution (weighted average of anion conductivities).

$$x_{OH^-} = \frac{[OH^-]}{[OH^-] + 2[CO_3^{2-}]} \tag{8}$$

The results indicate that the relation between the solution concentration and the membrane's conductivity is not linear, but rather increases exponentially. It means that while operating an AEMFC in which the membrane is initially carbonated, a large generation of OH^- is required in order to affect the conductivity in a significant way. However, deviation from the theoretical linear prediction could also indicate that there is a difference between CO_3^{2-} and OH^- absorbance into the membrane. The results of this calculation provide a higher conductivity value than the experimental data in most of the concentration range (up to ~ X_{OH} = 0.9), suggesting that the actual concentration of OH^- in the membrane is lower than the one in the solution. A similar conclusion was previously reached by Suzuki et al. by measuring anion concentration in an A201 AEM (Tokuyama, Japan), which was immersed in varying OH^-/CO_3^{2-} mixtures [41].

These results may explain the strong effect of even a small concentration of HCO_3^- and CO_3^{2-} in the AEM anion conductivity and on the AEMFC performance, as it was shown that OH^- concentration is higher than HCO_3^- and CO_3^{2-} during cell operation at moderate current densities [36]. Nevertheless, several experimental results confirm the lower AEMFC performance in cells running on ambient air as compared to those running on CO_2-free air [6,18,23,25,43,66].

As mentioned previously, during the startup process of the AEMFC, OH^- replaces the existing HCO_3^- and CO_3^{2-} and increases the effective AEM anion conductivity [22,36]. To simulate this transient phenomenon and study the transient values of conductivity during what we can call 'decarbonation' process or 'self-purging' process, a similar ex-situ process was studied experimentally by applying a constant continuous current through an AEM initially in its HCO_3^- form. In this method,

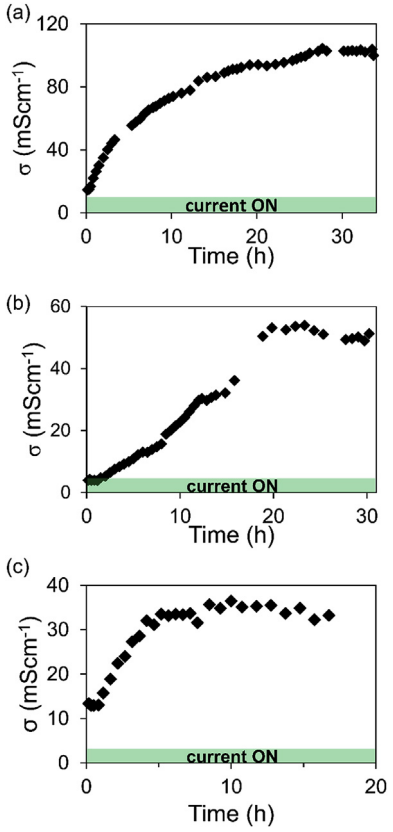

Fig. 11. Measurements of transient anion conductivity during in-situ OH^- formation in an AEM, for both (a) HMT-PMBI, (b) FAA-3 and (c) PPO-Im. Conditions: 500 mL/min N_2/N_2+CO_2 flow, 40 °C, 90% RH.

which was first explained in detail elsewhere [48], OH^- is produced in-situ in the AEM and at the same time CO_2 is (self)purged from the membrane in electrochemical reactions stimulated by the external current. This novel method was recently used to 'force' complete removal of the carbonation species (self-purge process) and measure the true (pure) OH^- conductivity in AEMs [48].

Fig. 11 presents the transient effective AEM anion conductivity values measured during application of this technique. For the three AEMs (HMT-PMBI, FAA-3 and PPO-Im), the effective anion conductivity increases significantly immediately after applying the external current through the AEM, and reaches a relatively stable value of ~100 mS/cm, ~50 mS/cm and ~35 mS/cm for the HMT-PMBI, FAA-3 and PPO-Im AEMs, respectively. These values are defined as the true OH^- conductivity of the AEMs [48]. The ratio between the membranes' OH^- conductivities is smaller compared to the conventional measurements performed using standard steady state conductivity measurements (see Fig. 3), suggesting that by using this novel technique, higher OH^- conductivity values are measured.

The time required for fully replacing HCO_3^- and CO_3^{2-} with OH^- is different for each AEM. For HMT-PMBI this time is ~30 h, for FAA-3 around 20 h and for PPO-Im it appears to be ca. 10 h. This difference can be explained by the differences in IEC of the membranes (2.5, ~1.7 and ~1.64 mmol/g, respectively). Since HMT-PMBI contains a larger initial concentration of HCO_3^-/CO_3^{2-} it requires more time to obtain a pure OH^- form. PPO-Im requires the shortest time to reach stable conductivity, however it has the lowest value of OH^- conductivity and also it might be affected by the ambient conditions; it is visible in Fig. 7 that PPO-Im OH^- conductivity is not stable at 90% RH and 40 °C over the course of 6 h, which could affect the measurement in this method.

Since the current density applied in this method is limited to 20 mA/cm^2 (due to practical instrumentation limitations), the time required to purge all HCO_3^- and CO_3^{2-} from the AEM is very long. For comparison, in a typical AEMFC the current density can reach above 1 A/cm^2 [37]. For such current densities, OH^- generation is significantly faster and therefore, this de-carbonation process can take place in much shorter time. As a quick estimation, assuming a linear relationship between the current applied and the rate of the de-carbonation process, using a current density of 1 A/cm^2 in this method would require ~40 min to obtain pure OH^- form HMT-PMBI AEM from the initially carbonated form. A similar process was described in an AEMFC model by Wrubel et al. [67] where carbonated AEM reaches OH^- conductivity after only ~4 min at a current density of 100 mA/cm^2.

4. Conclusions

AEMFCs are a highly attractive and promising technology. However, AEMFCs still face the challenge of performance reduction when they run under ambient air, due to the quick carbonation of the OH^- anions in the AEM. The carbonation process in AEMs was scarcely studied. In order to get a better understanding of this process, and find ways to overcome the carbonation effect on AEMFCs, extensive study of the effect of CO_2 on AEMs is necessary.

In this work, the conductivity and water uptake properties of different AEMs in their three main relevant anion forms (OH^-, HCO_3^- and CO_3^{2-}) were studied and compared. For the first time, the effect of CO_2 on the transient behavior of the AEMs in the three main anion forms was also presented and discussed. Transient effective conductivities during carbonation and de-carbonation process were measured by a new ex-situ conductivity technique, where OH^- anions are in-situ generated during conductivity measurements of the AEMs.

This work provides unique and important data on AEM properties under the effect of CO_2 and the products of the carbonation process (HCO_3^- and CO_3^{2-}). Further research in this field is needed to increase the understanding of the effect of CO_2 aiming to finally be able to design high performance AEMFCs running on ambient air.

Conflicts of interest

The authors declare no conflict of interest.

Acknowledgment

This work was partially funded by the Nancy & Stephan Grand Technion Energy Program (GTEP); by the European Union's Horizon 2020 research and innovation program [grant No. 721065]; by the Ministry of Science, Technology & Space of Israel through the M. Era-NET Transnational Call 2015, NEXTGAME project [grant No. 3-12940] and through grant No. 3-12948; by the Israel Science Foundation (ISF) [grant No. 1481/17]; by the Israel Innovation Authority through the KAMIN program [grant No. 60503]; and by the Ministry of National Infrastructure, Energy and Water Resources of Israel [grant No. 3-13671]. The authors would also like to acknowledge the financial support of Melvyn & Carolyn Miller Fund for Innovation, as well as the support of Planning & Budgeting Committee / ISRAEL Council for Higher Education (CHE) and Fuel Choice Initiative (Prime Minister Office of ISRAEL), within the framework of "Israel National Research Center for Electrochemical Propulsion".

Appendix A. Supplementary data

Supplementary data to this article can be found online at https://doi.org/10.1016/j.memsci.2019.05.053.

References

[1] J.R. Varcoe, P. Atanassov, D.R. Dekel, A.M. Herring, M.A. Hickner, P.A. Kohl, A.R. Kucernak, W.E. Mustain, K. Nijmeijer, K. Scott, T. Xu, L. Zhuang, Anion-

exchange membranes in electrochemical energy systems, Energy Environ. Sci. 7 (2014) 3135–3191, https://doi.org/10.1039/C4EE01303D.
[2] H.A. Miller, A. Lavacchi, F. Vizza, M. Marelli, F. Di Benedetto, F. D'Acapito, Y. Paska, M. Page, D.R. Dekel, A Pd/C-CeO 2 anode catalyst for high-performance platinum-free anion exchange membrane fuel cells, Angew. Chem. 128 (2016) 6108–6111, https://doi.org/10.1002/ange.201600647.
[3] T.J. Omasta, X. Peng, H.A. Miller, F. Vizza, L. Wang, J.R. Varcoe, D.R. Dekel, W.E. Mustain, Beyond 1.0 W cm −2 performance without platinum: the beginning of a new era in anion exchange membrane fuel cells, J. Electrochem. Soc. 165 (2018) J3039–J3044, https://doi.org/10.1149/2.0071815jes.
[4] M. Alesker, M. Page, M. Shviro, Y. Paska, G. Gershinsky, D.R. Dekel, D. Zitoun, Palladium/nickel bifunctional electrocatalyst for hydrogen oxidation reaction in alkaline membrane fuel cell, J. Power Sources 304 (2016) 332–339, https://doi.org/10.1016/j.jpowsour.2015.11.026.
[5] H.A. Miller, F. Vizza, M. Marelli, A. Zadick, L. Dubau, M. Chatenet, S. Geiger, S. Cherevko, H. Doan, R.K. Pavlicek, S. Mukerjee, D.R. Dekel, Highly active nanostructured palladium-ceria electrocatalysts for the hydrogen oxidation reaction in alkaline medium, Nano Energy 33 (2017) 293–305, https://doi.org/10.1016/j.nanoen.2017.01.051.
[6] M. Piana, M. Boccia, A. Filpi, E. Flammia, H.A. Miller, M. Orsini, F. Salusti, S. Santiccioli, F. Ciardelli, A. Pucci, H2/air alkaline membrane fuel cell performance and durability, using novel ionomer and non-platinum group metal cathode catalyst, J. Power Sources 195 (2010) 5875–5881, https://doi.org/10.1016/j.jpowsour.2009.12.085.
[7] Q. Hu, G. Li, J. Pan, L. Tan, J. Lu, L. Zhuang, Alkaline polymer electrolyte fuel cell with Ni-based anode and Co-based cathode, Int. J. Hydrogen Energy 38 (2013) 16264–16268, https://doi.org/10.1016/j.ijhydene.2013.09.125.
[8] A. Sarapuu, E. Kibena-Põldsepp, M. Borghei, K. Tammeveski, Electrocatalysis of oxygen reduction on heteroatom-doped nanocarbons and transition metal–nitrogen–carbon catalysts for alkaline membrane fuel cells, J. Mater. Chem. A. 6 (2018) 776–804, https://doi.org/10.1039/C7TA08690C.
[9] M.M. Hossen, K. Artyushkova, P. Atanassov, A. Serov, Synthesis and characterization of high performing Fe-N-C catalyst for oxygen reduction reaction (ORR) in Alkaline Exchange Membrane Fuel Cells, J. Power Sources 375 (2018) 214–221, https://doi.org/10.1016/j.jpowsour.2017.08.036.
[10] H. Yu, E.S. Davydova, U. Ash, H.A. Miller, L. Bonville, D.R. Dekel, R. Maric, Palladium-ceria nanocatalyst for hydrogen oxidation in alkaline media: optimization of the Pd–CeO2 interface, Nano Energy 57 (2019) 820–826, https://doi.org/10.1016/j.nanoen.2018.12.098.
[11] L.A. Adams, S.D. Poynton, C. Tamain, R.C.T. Slade, J.R. Varcoe, A carbon dioxide tolerant aqueous-electrolyte-free anion-exchange membrane alkaline fuel cell, ChemSusChem 1 (2008) 79–81, https://doi.org/10.1002/cssc.200700013.
[12] C. Lafforgue, M. Chatenet, L. Dubau, D.R. Dekel, Accelerated stress test of Pt/C nanoparticles in an interface with an anion-exchange membrane—an identical-location transmission electron microscopy study, ACS Catal. 8 (2018) 1278–1286, https://doi.org/10.1021/acscatal.7b04055.
[13] D.R. Dekel, M. Amar, S. Willdorf, M. Kosa, S. Dhara, C.E. Diesendruck, Effect of water on the stability of quaternary ammonium groups for anion exchange membrane fuel cell applications, Chem. Mater. 29 (2017) 4425–4431, https://doi.org/10.1021/acs.chemmater.7b00958.
[14] D.R. Dekel, S. Willdorf, U. Ash, M. Amar, S. Pusara, S. Dhara, S. Srebnik, C.E. Diesendruck, The critical relation between chemical stability of cations and water in anion exchange membrane fuel cells environment, J. Power Sources 375 (2018) 351–360, https://doi.org/10.1016/j.jpowsour.2017.08.026.
[15] C.E. Diesendruck, D.R. Dekel, Water – a key parameter in the stability of anion exchange membrane fuel cells, Curr. Opin. Electrochem. 9 (2018) 173–178, https://doi.org/10.1016/j.coelec.2018.03.019.
[16] M.G. Marino, K.D. Kreuer, Alkaline stability of quaternary ammonium cations for alkaline fuel cell membranes and ionic liquids, ChemSusChem 8 (2015) 513–523, https://doi.org/10.1002/cssc.201403022.
[17] A. Amel, S.B. Smedley, D.R. Dekel, M.A. Hickner, Y. Ein-Eli, Characterization and chemical stability of anion exchange membranes cross-linked with polar electron-donating linkers, J. Electrochem. Soc. 162 (2015) F1047–F1055, https://doi.org/10.1149/2.0891509jes.
[18] S. Gottesfeld, D.R. Dekel, M. Page, C. Bae, Y. Yan, P. Zelenay, Y.S. Kim, Anion exchange membrane fuel cells: current status and remaining challenges, J. Power Sources 375 (2018) 170–184, https://doi.org/10.1016/j.jpowsour.2017.08.010.
[19] S. Pusara, S. Srebnik, D.R. Dekel, Molecular simulation of quaternary ammonium solutions at low hydration levels, J. Phys. Chem. C 122 (2018) 11204–11213, https://doi.org/10.1021/acs.jpcc.8b00752.
[20] S. Willdorf-Cohen, A.N. Mondal, D.R. Dekel, C.E. Diesendruck, Chemical stability of poly(phenylene oxide)-based ionomers in an anion exchange-membrane fuel cell environment, J. Mater. Chem. A. 6 (2018) 22234–22239, https://doi.org/10.1039/C8TA05785K.
[21] E.S. Davydova, S. Mukerjee, F. Jaouen, D.R. Dekel, Electrocatalysts for hydrogen oxidation reaction in alkaline electrolytes, ACS Catal. 8 (2018) 6665–6690, https://doi.org/10.1021/acscatal.8b00689.
[22] N. Ziv, W.E. Mustain, D.R. Dekel, The effect of ambient carbon dioxide on anion-exchange membrane fuel cells, ChemSusChem 11 (2018) 1136–1150, https://doi.org/10.1002/cssc.201702330.
[23] G. Li, Y. Wang, J. Pan, J. Han, Q. Liu, X. Li, P. Li, C. Chen, L. Xiao, J. Lu, L. Zhuang, Carbonation effects on the performance of alkaline polymer electrolyte fuel cells, Int. J. Hydrogen Energy 40 (2015) 6655–6660, https://doi.org/10.1016/j.ijhydene.2015.03.119.
[24] L. Topal, C. Nunes Kirchner, W. Germer, M. Zobel, A. Dyck, Evaluation of cathode gas composition and temperature influences on alkaline anion exchange membrane fuel cell (AAEMFC) performance, Int. J. Renew. Energy Dev. 3 (2014) 65–72, https://doi.org/10.14710/ijred.3.1.65-72.
[25] K. Fukuta, H. Inoue, S. Watanabe, H. Yanagi, In-situ observation of CO2 through the self-purging in alkaline membrane fuel cell (AMFC), ECS Trans 19 (2009) 23–27, https://doi.org/10.1149/1.3271358.
[26] E.R. Nightingale, Phenomenological theory of ion solvation. Effective radii of hydrated ions, J. Phys. Chem. 63 (1959) 1381–1387, https://doi.org/10.1021/j150579a011.
[27] B.W. Connors, B.R. Ransom, Chloride conductance and extracellular potassium concentration interact to modify the excitability of rat optic nerve fibres, J. Physiol. 355 (1984) 619–633, https://doi.org/10.1113/jphysiol.1984.sp015442.
[28] A.M. Kiss, T.D. Myles, K.N. Grew, A.A. Peracchio, G.J. Nelson, W.K.S. Chiu, Carbonate and bicarbonate ion transport in alkaline anion exchange membranes, J. Electrochem. Soc. 160 (2013) F994–F999, https://doi.org/10.1149/2.037309jes.
[29] K.N. Grew, D. Chu, W.K.S. Chiu, Ionic equilibrium and transport in the alkaline anion exchange membrane, J. Electrochem. Soc. 157 (2010) B1024, https://doi.org/10.1149/1.3368728.
[30] K.N. Grew, W.K.S. Chiu, A dusty fluid model for predicting hydroxyl anion conductivity in alkaline anion exchange membranes, J. Electrochem. Soc. 157 (2010) B327, https://doi.org/10.1149/1.3273200.
[31] M.E. Tuckerman, D. Marx, M. Parrinello, The nature and transport mechanism of hydrated hydroxide ions in aqueous solution, Nature 417 (2002) 925–929, https://doi.org/10.1038/nature00797.
[32] J.A. Vega, C. Chartier, W.E. Mustain, Effect of hydroxide and carbonate alkaline media on anion exchange membranes, J. Power Sources 195 (2010) 7176–7180, https://doi.org/10.1016/j.jpowsour.2010.05.030.
[33] S. Watanabe, K. Fukuta, H. Yanagi, Determination of carbonate ion in MEA during the alkaline membrane fuel cell (AMFC) operation, ECS Trans 33 (2010) 1837–1845, https://doi.org/10.1149/1.3484674.
[34] Z. Siroma, S. Watanabe, K. Yasuda, K. Fukuta, H. Yanagi, Mathematical modeling of the concentration profile of carbonate ions in an anion exchange membrane fuel cell, J. Electrochem. Soc. 158 (2011) B682, https://doi.org/10.1149/1.3576120.
[35] H. Yanagi, K. Fukuta, Anion exchange membrane and ionomer for alkaline membrane fuel cells (AMFCs), ECS Trans 16 (2008) 257–262, https://doi.org/10.1149/1.2981860.
[36] U. Krewer, C. Weinzierl, N. Ziv, D.R. Dekel, Impact of carbonation processes in anion exchange membrane fuel cells, Electrochim. Acta 263 (2018) 433–446, https://doi.org/10.1016/j.electacta.2017.12.093.
[37] D.R. Dekel, Review of cell performance in anion exchange membrane fuel cells, J. Power Sources 375 (2018) 158–169, https://doi.org/10.1016/j.jpowsour.2017.07.117.
[38] J. Peng, A.L. Roy, S.G. Greenbaum, T.A. Zawodzinski, Effect of CO 2 absorption on ion and water mobility in an anion exchange membrane, J. Power Sources 380 (2018) 64–75, https://doi.org/10.1016/j.jpowsour.2018.01.071.
[39] A.G. Divekar, A.M. Park, Z.R. Owczarczyk, S. Seifert, B.S. Pivovar, A.M. Herring, A study of carbonate formation kinetics and morphological effects observed on OH - form of Pfaem when exposed to air containing CO 2, ECS Trans 80 (2017) 1005–1011, https://doi.org/10.1149/08008.1005ecst.
[40] T.P. Pandey, B.D. Peters, M.W. Liberatore, A.M. Herring, Insight on pure vs air exposed hydroxide ion conductivity in an anion exchange membrane for fuel cell applications, ECS Trans 64 (2014) 1195–1200, https://doi.org/10.1149/06403.1195ecst.
[41] S. Suzuki, H. Muroyama, T. Matsui, K. Eguchi, Influence of CO_2 dissolution into anion exchange membrane on fuel cell performance, Electrochim. Acta 88 (2013) 552–558, https://doi.org/10.1016/j.electacta.2012.10.105.
[42] A.G. Divekar, B.S. Pivovar, A.M. Herring, Kinetic equilibrium study of CO 2 Poisoning observed in anion exchange membranes when exposed to ambient air and varying levels of CO 2 ppm, ECS Trans 86 (2018) 643–648, https://doi.org/10.1149/08613.0643ecst.
[43] A.G. Wright, J. Fan, B. Britton, T. Weissbach, H.-F. Lee, E.A. Kitching, T.J. Peckham, S. Holdcroft, Hexamethyl-p-terphenyl poly(benzimidazolium): a universal hydroxide-conducting polymer for energy conversion devices, Energy Environ. Sci. 9 (2016) 2130–2142, https://doi.org/10.1039/C6EE00656F.
[44] A.G. Wright, S. Holdcroft, Hydroxide-stable ionenes, ACS Macro Lett. 3 (2014) 444–447, https://doi.org/10.1021/mz500168d.
[45] Y. Zheng, U. Ash, R.P. Pandey, A.G. Ozioko, J. Ponce-González, M. Handl, T. Weissbach, J.R. Varcoe, S. Holdcroft, M.W. Liberatore, R. Hiesgen, D.R. Dekel, Water uptake study of anion exchange membranes, Macromolecules 51 (2018) 3264–3278, https://doi.org/10.1021/acs.macromol.8b00034.
[46] Technical data sheet fumapem FAA-3-30, (n.d.).
[47] K.R. Cooper, Characterizing through-plane and in-plane ionic conductivity of polymer electrolyte membranes, ECS Trans 41 (2011) 1371–1380, https://doi.org/10.1149/1.3635668.
[48] N. Ziv, D.R. Dekel, A practical method for measuring the true hydroxide conductivity of anion exchange membranes, Electrochem. Commun. 88 (2018) 109–113, https://doi.org/10.1016/j.elecom.2018.01.021.
[49] E. Drioli, L. Giorno, Comprehensive Membrane Science and Engineering, Elsevier Science, 2010, https://www.sciencedirect.com/science/referenceworks/9780080932507#ancv0010 , Accessed date: 9 May 2018.
[50] D. Aili, A.G. Wright, M.R. Kraglund, K. Jankova, S. Holdcroft, J.O. Jensen, Towards a stable ion-solvating polymer electrolyte for advanced alkaline water electrolysis, J. Mater. Chem. A. 5 (2017) 5055–5066, https://doi.org/10.1039/C6TA10680C.
[51] J. Fan, A.G. Wright, B. Britton, T. Weissbach, T.J.G. Skalski, J. Ward, T.J. Peckham, S. Holdcroft, Cationic Polyelectrolytes, stable in 10 M KOH aq at 100 °C, ACS Macro Lett. 6 (2017) 1089–1093, https://doi.org/10.1021/acsmacrolett.7b00679.
[52] D.R. Dekel, I.G. Rasin, M. Page, S. Brandon, Steady state and transient simulation of

anion exchange membrane fuel cells, J. Power Sources 375 (2018) 191–204, https://doi.org/10.1016/j.jpowsour.2017.07.012.
[53] M.G. Marino, J.P. Melchior, A. Wohlfarth, K.D. Kreuer, Hydroxide, halide and water transport in a model anion exchange membrane, J. Membr. Sci. 464 (2014) 61–71, https://doi.org/10.1016/j.memsci.2014.04.003.
[54] E.M. Schibli, A.G. Wright, S. Holdcroft, B.J. Frisken, Morphology of anion-conducting ionenes investigated by X-ray scattering and simulation, J. Phys. Chem. B 122 (2018) 1730–1737, https://doi.org/10.1021/acs.jpcb.7b10177.
[55] X. Luo, A. Wright, T. Weissbach, S. Holdcroft, Water permeation through anion exchange membranes, J. Power Sources 375 (2018) 442–451, https://doi.org/10.1016/j.jpowsour.2017.05.030.
[56] P.M. Mangiagli, C.S. Ewing, K. Xu, Q. Wang, M. a. Hickner, Dynamic water uptake of flexible ion-containing polymer networks, Fuel Cells 9 (2009) 432–438, https://doi.org/10.1002/fuce.200800157.
[57] S.K. Burgess, D.S. Mikkilineni, D.B. Yu, D.J. Kim, C.R. Mubarak, R.M. Kriegel, W.J. Koros, Water sorption in poly(ethylene furanoate) compared to poly(ethylene terephthalate). Part 1: equilibrium sorption, Polymer 55 (2014) 6861–6869, https://doi.org/10.1016/J.POLYMER.2014.10.047.
[58] T. Kimura, R. Akiyama, K. Miyatake, J. Inukai, Phase separation and ion conductivity in the bulk and at the surface of anion exchange membranes with different ion exchange capacities at different humidities, J. Power Sources 375 (2018) 397–403 https://doi.org/10.1016/j.jpowsour.2017.06.081 http://linkinghub.elsevier.com/retrieve/pii/S0378775317308649 , Accessed date: 5 September 2017.
[59] A. Amel, N. Gavish, L. Zhu, D.R. Dekel, M.A. Hickner, Y. Ein-Eli, Bicarbonate and chloride anion transport in anion exchange membranes, J. Membr. Sci. 514 (2016) 125–134, https://doi.org/10.1016/j.memsci.2016.04.027.
[60] K.N. Grew, X. Ren, D. Chu, Effects of temperature and carbon dioxide on anion exchange membrane conductivity, Electrochem. Solid State Lett. 14 (2011) B127, https://doi.org/10.1149/2.011112esl.
[61] A.G. Wright, T. Weissbach, S. Holdcroft, Poly(phenylene) and m -terphenyl as powerful protecting groups for the Preparation of stable organic hydroxides, Angew. Chem. Int. Ed. 55 (2016) 4818–4821, https://doi.org/10.1002/anie.201511184.
[62] I.G. Rasin, M. Page, D.R. Dekel, S. Brandon, A model based analysis of alkaline membrane fuel cells, ECS Trans 80 (2017) 1051–1057, https://doi.org/10.1149/08008.1051ECST.
[63] A.M. Maes, T.P. Pandey, M.A. Vandiver, L.K. Lundquist, Y. Yang, J.L. Horan, A. Krosovsky, M.W. Liberatore, S. Seifert, A.M. Herring, Preparation and characterization of an alkaline anion exchange membrane from chlorinated poly(propylene) aminated with branched poly(ethyleneimine), Electrochim. Acta 110 (2013) 260–266, https://doi.org/10.1016/j.electacta.2013.04.033.
[64] J. Kizewski, N. Mudri, R. Zeng, S. Poynton, R.C.T. Slade, J.R. Varcoe, Alkaline electrolytes and reference electrodes for alkaline polymer electrolyte membrane fuel cells, ECS Trans 33 (2010) 27–35, https://doi.org/10.1149/1.3484498.
[65] T.D. Myles, K.N. Grew, A.A. Peracchio, W.K.S. Chiu, Transient ion exchange of anion exchange membranes exposed to carbon dioxide, J. Power Sources 296 (2015) 225–236, https://doi.org/10.1016/j.jpowsour.2015.07.044.
[66] M. Inaba, Y. Matsui, M. Saito, A. Tasaka, K. Fukuta, S. Watanabe, H. Yanagi, Effects of carbon dioxide on the performance of anion-exchange membrane fuel cells, Electrochemistry 79 (2011) 322–325, https://doi.org/10.5796/electrochemistry.79.322.
[67] J.A. Wrubel, A.A. Peracchio, B.N. Cassenti, T.D. Myles, K.N. Grew, W.K.S. Chiu, Anion exchange membrane ionic conductivity in the presence of carbon dioxide under fuel cell operating conditions, ECS Trans 80 (2017) 989–1003, https://doi.org/10.1149/08008.0989ecst.